Geophysical and hydrogeological survey in a part of the Nhandugue River valley, Gorongosa National Park, Mozambique -Area 2 and 3

Kristina Arvidsson

**Dissertations in Geology at Lund University,
Master's thesis, no 256
(45 hp/ECTS credits)**

Minor Field Studies (MFS) Scholarship Programme

**Department of Earth- and Ecosystem Sciences
Division of Geology
Lund University**
2010

LUNDS TEKNISKA HÖGSKOLA
Lunds universitet

Lund University
Faculty of Engineering, LTH
Departments of Earth and Water Engineering

This study has been carried out within the framework of the Minor Field Studies (MFS) Scholarship Programme, which is funded by the Swedish International Development Cooperation Agency, Sida.

The MFS Scholarship Programme offers Swedish university students an opportunity to carry out two months' field work in a developing country resulting in a graduation thesis work, a Master's dissertation or a similar in-depth study. These studies are primarily conducted within subject areas that are important from an international development perspective and in a country supported by Swedish international development assistance.

The main purpose of the MFS Programme is to enhance Swedish university students' knowledge and understanding of developing countries and their problems. An MFS should provide the student with initial experience of conditions in such a country. A further purpose is to widen the human resource base for recruitment into international co-operation. Further information can be reached at the following internet address: http://www.tg.lth.se/mfs.

The responsibility for the accuracy of the information presented in this MFS report rests entirely with the authors and their supervisors.

Gerhard Barmen
Local MFS Programme Officer

Postadress Box 118, 221 00 Lund *Besöksadress* John Ericssons väg 1*Telefon dir* 046-222 9657, *växel* 046-222 00 00 *Telefax* 046-2229127
E-post Gerhard.Barmen@tg.lth.se

Geophysical and hydrogeological survey in a part of the Nhandugue River valley, Gorongosa National Park, Mozambique

- Area 2 and 3

Master Thesis

Kristina Arvidsson

Department of Earth and Ecosystem Sciences
Division of Geology
Lund University
2010

Contents

Cover Picture: Section of the Nhandugue River, Gorongosa National Park, Mozambique. Photo by Kristina Arvidsson.

Contents

Geophysical and hydrogeological survey in a part of the Nhandugue River valley, Gorongosa National Park, Mozambique — Area 2 and 3

KRISTINA ARVIDSSON

Arvidsson, K., 2010: Geophysical and hydrogeological survey in a part of the Nhandugue River valley, Gorongosa National Park, Mozambique — Area 2 and 3. *Examensarbeten i geologi vid Lunds universitet*, Nr. 256, 36 pp. 45 ECTS credits.

Abstract: Gorongosa National Park in central Mozambique is situated at the southernmost extension of the East African Rift System (EARS), the Urema Rift. The park is protecting a vast ecosystem of floodplains, grasslands and woody coverage. From 20 years of civil war the large-mammal population in the park had in year 1994 been reduced by 90 % or more, and in 2004 a restoration project was started in order to rebuild and rehabilitate the park. For an ecosystem in balance, water resources are indispensable and Lake Urema in the central part of the park is vital. In order to maintain a sound management and decision-making about water resources in the Gorongosa region park authorities want to predict the hydrological effects due to changes in different environmental factors. For this, new and additional information is needed about the hydrogeological conditions of the park.

Focus in this paper is to provide hydrogeological information about the western margin of the Urema Rift, since it has been anticipated that this area is a potential major groundwater recharge zone to the deeper Rift valley floor sediments. The methods used in the study are resistivity and induced polarisation (IP) measurements, together with geological ground truthing and discharge measurements. Data were collected from three areas (Area 1-3) along the Nhandugue River at the north-western border of the park. In this paper the results from Area 2 and 3 are presented, whereas the data from Area 1 is presented in a paper by Stenberg (2010).

Three layers of Quaternary alluvial sediments and one bottommost layer of sandstone can be identified in the resistivity models. Soil samples show variations in grain sizes and mineralogical composition depending on where in the river valley the material was deposited. A topmost unconfined aquifer is identified, below which there is a partly permeable aquiclude in turn covering two different semi-confined aquifers. A downstream water loss in the Nhandugue River suggests that surface water infiltrates to the deeper aquifers and is transported as groundwater in an east/southeast-ward direction. The hydrogeological conditions confirm that the rift margin is a likely groundwater recharge zone and the east/southeast-ward hydraulic groundwater gradient indicate that groundwater is flowing towards, and feeds, Lake Urema.

Keywords: Mozambique, geophysical methods, groundwater, Urema Rift, Gorongosa National Park, Nhandugue River.

Kristina Arvidsson, Department of Earth and Ecosystem Sciences, Division of Geology, GeoBiosphere Science Centre, Lund University, Sölvegatan 12, SE-223 62 Lund, Sweden. E-mail: kristina.arvidsson@gmail.com

Geofysisk och hydrogeologisk undersökning i en del av Nhandugue-flodens floddal, Gorongosa Nationalpark, Moçambique — Område 2 och 3

KRISTINA ARVIDSSON

Arvidsson, K., 2010: Geophysical and hydrogeological survey in a part of the Nhandugue River valley, Gorongosa National Park, Mozambique — Område 2 and 3. *Examensarbeten i geologi vid Lunds universitet*, Nr. 256, 36 sid. 45 hp.

Sammanfattning: Gorongosa Nationalpark i centrala Moçambique ligger i den sydligaste delen av det Östafrikanska riftsystemet, Urema-riften. Parken ger skydd ett omfattande ekosystem av flodplan, gräsmark och skogsbeklädda områden. Efter 20 år av inbördeskrig hade populationen av stora däggdjur år 1994 minskat med 90 % eller mer och under 2004 påbörjades ett restaureringsprojekt för att återuppbygga och återställa parken. För att ekosystemet ska fungera är vattenresurserna ovärderliga och Urema-sjön i den centrala delen av parken är livsnödvändig. För att bibehålla en hållbar hantering av och beslutsfattning kring vattenresurserna i Gorongosaregionen vill parkmyndigheterna kunna förutse de hydrologiska effekterna av förändringar i miljöbetingade faktorer. För att göra detta behövs mer och ny information om de hydrogeologiska förhållandena.

Fokus i denna uppsats ligger på att ta fram information rörande den västra kanten av Urema-riften, då det har antagits att detta område är en potentiell betydande grundvattenbildningszon till de djupare liggande riftdalssedimenten. De metoder som har använts i studien är resistivitets- och inducerad polarisations (IP)- mätningar, tillsammans med geologisk fältkontroll och avrinningsmätningar. Data samlades in från tre områden (1-3) längs Nhandugue-floden som flyter längs med den nordvästra parkgränsen. Presenterat i denna uppsats är resultaten från område 2 och 3, medan resultaten från område 1 presenteras i en uppsats av Stenberg (2010).

Tre lager av kvartära alluviala sediment och ett undre lager av sandsten kan identifieras i resistivitetsmodellerna. Jordproverna visar att kornstorlek och mineralogisk sammansättning varierar beroende på var i floddalen materialet har avsatts. Från markytan och neråt kan en öppen akvifär, en delvis permeabel akviklud och två olika semi-slutna akvifärer urskiljas. En nedströms förlust av vatten i Nhandugue-floden indikerar att ytvatten infiltrerar till de djupare liggande akvifärerna och transporteras som grundvatten i en öst/sydöstlig riktning. De hydrogeologiska förhållandena bekräftar att riftkanten är en trolig grundvattenbildningszon och den öst/sydöstliga hydrauliska grundvattengradienten indikerar att det är möjligt att grundvatten flödar mot och tillför vatten till Urema-sjön.

Nyckelord: Moçambique, geofysiska metoder, grundvatten, Urema-riften, Gorongosa Nationalpark, Nhandugue-floden.

Kristina Arvidsson, Institutionen för geo– och ekosystemvetenskaper, Enheten för geologi, Centrum för GeoBiosfärsvetenskap, Lunds Universitet, Sölvegatan 12, 223 62 Lund, Sverige. E-post: kristina.arvidsson@gmail.com

1 Introduction

Gorongosa National Park (GNP) in central Mozambique is situated at the southernmost extension of the East African Rift System (EARS), the Urema Rift. The park is protecting a vast ecosystem of floodplains, grasslands and woody coverage (Beilfuss *et al.* 2007). For the function of this ecosystem, water resources are indispensable. Several rivers, among these the Nhandugue River, are flowing into the park and merges in Lake Urema in the central part of the park. This lake is vital for GNP, and park authorities want to predict the effects of changes in different environmental factors, in order to maintain a sound management and decision-making about water resources in the Gorongosa region (Beilfuss *et al.* 2007). To obtain this, more information is needed about the geology and hydrology in the area.

In 2007 the Gorongosa Research Center prepared the plan *Long-term plan for hydrological research: adaptive management of water resources at Gorongosa National park* (Beilfuss *et al.* 2007). During an expert meeting in the same year it was suggested to conduct a multi-resistivity survey, thereby obtaining two-dimensional images of the subsurface across the Urema Rift. The first geophysical survey was conducted in 2008 by Farisse Chirindja and Kristofer Hellman (Chirindja & Hellman 2009) as part of a SIDA-SAREC funded research cooperation between Lund University, Eduardo Mondlane University and GNP. An evaluation of the results suggested further surveys with additional resistivity profiles. A recommendation was also to collect reference data to improve the reliability of the interpretation of the profiles.

This paper is focusing on the western rift margin since it has been anticipated that this area is a potential major groundwater recharge zone to the deeper Rift valley floor sediments. The Nhandugue River is a seasonal sand river which rises from outside the park and crosses the park boundary in the north-western corner (Tinley 1977). It was decided to pay special attention to the area where the Nhandugue River flows from the basement gneisses across the fault margin and onto the Rift valley floor sedimentary fill. The purpose of this paper is to provide new and additional information about the hydrogeological conditions of this setting. Field work was conducted as part of the SIDA-SAREC funded research cooperation between Lund University, Eduardo Mondlane University and GNP and was conducted together with Li Stenberg, Farisse Chirindja, Luís Magaia and Felix Oqueio in June to August 2009. Data were collected from three different areas along the river (Areas 1-3). The results are presented and interpreted in two separate papers, Area 1 and the transition to Area 2 treated by Li Stenberg (Stenberg 2010), while the present paper focus on Area 2 and the transition to the downstream Area 3. The questions to be answered are:

- How thick are the Quaternary sediments and in what environment where they deposited?
- What changes can be seen in the sediments (grain size, mineralogy and carbonate content), going downstream from Area 2 to 3?
- Is the Sena Formation underlying the sediments? If so, in what way could it influence the hydraulic conditions?
- What aquifers and aquicludes/aquitards are present? What are the extents of these?
- What is the amount of surface water discharge? Is it changing downstream?
- What possible routings are there for surface and groundwater flow? Is there a possibility for water to infiltrate to deeper aquifers?
- Is there a possibility for groundwater recharge?

2 Background

Gorongosa National Park is situated at 19°S and 34°W, within the Sofala province in the central part of Mozambique (Fig. 1). The morphology of the central Mozambican landscape is rising inland, from a broad shallow continental shelf and a low coast line, to the Great Eastern Escarpment on the border between Mozambique and Zimbabwe (Tinley 1977). The park is situated within the Urema Rift and covers an area of approximately 3770 km^2. The park together with the

Fig. 1. A map showing the southern and central parts of Mozambique. Gorongosa National Park is located within the Sofala province, in the central part of Mozambique, and is marked with green. The map is modified from GNP (2009).

surrounding areas comprises four morphological units, which are from east to west; the Cheringoma Platform, the Rift valley floor, the Báruè Platform and the Gorongosa Mountain (Fig. 2; Tinley 1977).

2.1 History and restoration project

The Portuguese began colonising Mozambique in the early 16th century and held it until 1975, when Mozambique became independent (Halkjaer 2007). In 1960 the Portuguese government declared Gorongosa a National Park, and even though a war was going on for 11 years between 1964 and 1975, the park was experiencing a golden era in the years 1960-1980 (Gorongosa National Park [GNP] 2009). In 1981 a civil war began, and this time the park was put out to much damage. After attacks and kidnappings of park staff, the park was closed down in 1983. During the war large numbers of animals were killed, both by soldiers and by people who sought refuge in the park. The war ended in 1992, but widespread hunting continued for two more years. In 1994 the large-mammal population had been reduced by 90 % or more (GNP 2009).

After the war ended the African Development Bank, in cooperation with the European Union and International Union for the Conservation of Nature, started to rehabilitate GNP. In 2004 the Carr Foundation and the government of Mozambique agreed to continue the work on rebuilding the park. In 2007 a 6000-hectare wildlife sanctuary had been built and reconstruction of the Chitengo Safari Camp had begun. These initial years were a success and in 2008 it was announced that the government and the Carr Foundation had agreed to continue the restoration and co-management of the park for the coming 20 years (GNP 2009).

One feature of the restoration project is the *Long-term plan for hydrological research: adaptive management of water resources at Gorongosa National park* (Beilfuss *et al.* 2007). For protection of the park ecosystem water resources are fundamental and thus an important research object in connection with the work of restoring GNP (Beilfuss et al 2007).

2.2 Geological settings

2.2.1 Geological and tectonic development of Mozambique

To describe the geological development of Mozambique it is necessary to look at the development of the entire southern African region. During the Eoarchean and Paleoarchean (4000-3200 Ma), crustal formation and development took place and it was at this time the Gondwana supercontinent was formed (Lächelt 2004).

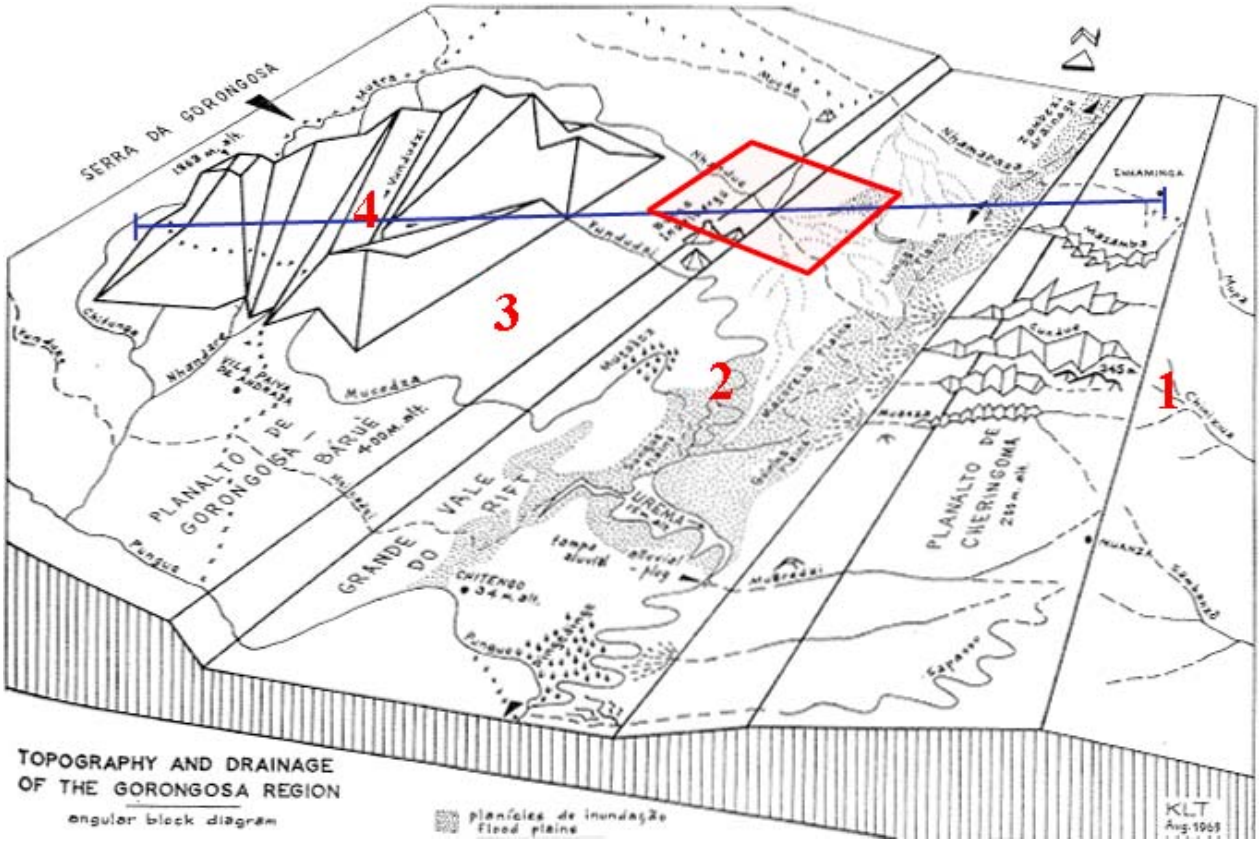

Fig. 2. Block model over the four morphological units present in the Gorongosa region. The four units are from east to west the Cheringoma Platform (1), the Rift valley floor (2), the Báruè Platform (3) and the Gorongosa Mountain (4). The blue line marks the location of the vertical geological cross-section in figure 3 and the read rectangle marks the part of the Nhandugue River valley where field work was conducted. The figure is adapted from Tinley (1977).

The following Mesoarchean and Neoarchean eras (3200-2500 Ma) were characterised by formation of a cratonic cover, granite-greenstone belts and a development of intracratonic mobile belts. Several tectonic cycles then took place during the Proterozoic (2500-542 Ma), ended with the Pan-African-Early Palaeozoic Cycle (In Mozambique: 850-410 Ma) (Lächelt 2004).

When the tectonic activity decreased in the early Palaeozoic the development continued with denudation and formation of local terrigenous sedimentary basins (Lächelt 2004). In the Late Palaeozoic-Early Mesozoic the activity increased again, and during the Karoo Period (300-157 Ma) sedimentary basins, depressions and rifts formed, coupled to volcanic eruptions forming the Karoo Supergroup. Corresponding to the Karoo Period is the Gondwana Period (300-157 Ma), which can be subdivided into the Gondwana Rifting Phase (300-205 Ma; Upper Carboniferous to Upper Triassic) and the Final Phase (205-157 Ma; Lower to Middle Jurassic) (Lächelt 2004). During the first phase, rift structures and platform depressions developed and were filled with mostly terrigenous sediments. In the second phase ocean margin basins, rifts and rift-accompanied structures were formed (Lächelt 2004). Magmatism was also active and basalt lavas formed vast lava plains, covering the low relief formed by the Karoo desert-like formations (Tinley 1977). At the end of Jurassic, denudation and sedimentary processes had cut across many geological formations and the landscape was reduced to a vast planation surface (Tinley 1977).

At the end of Jurassic and in the early Cretaceous the large break-up of Gondwanaland was initiated (Tinley 1977). This Post-Gondwana (Post-Karoo) Period (157 Ma to recent) can be divided into the three phases; (i) disintegration of the Gondwana Supercontinent (157-118 Ma), (ii) stabilization (118-35 Ma) and, (iii) neorifting (35 Ma to recent) (Lächelt 2004). During the first phase active seafloor spreading took place in the Mozambique Channel and Mozambique Basin. By this the Gondwana Supercontinent was divided into two regions. The western part comprised Africa and South America, while the eastern part consisted of what today are Antarctica, India, Sri Lanka, Madagascar, the Seychelles and Australia (Lächelt 2004). The second phase was characterised by another expansion of the continental margin basins, subsequently leading to detachment of Madagascar from India and the Seychelles. In the third phase, active tectonic movements resulted in formation of grabens and, most importantly, the formation of the East African Rift System (EARS). In addition to tectonic activity this phase was also characterised by thick sedimentation.

During the Quaternary, rifting and basin development continued and shallow-water shelf sediments were uplifted. They were by that exposed at the surface during the Holocene and the Gondwana planation surface was eroded (Tinley 1977).

2.2.2 Local geology

The Urema Rift, which comprises the most southern extent of the EARS, is a 40 km wide rift valley. Sets of NNE-SSW and NNW-SSE orientated faults and fracture zones on both sides of the valley (Tinley 1977) are responsible for the system of half-grabens that constitute the Urema Rift. A schematic vertical cross-section of the Urema Rift can be seen in figure 3. On the eastern side the valley is defined by the Cheringoma Platform and on the western side it is bounded by the Báruè Platform. Rising west of the Báruè Platform is the Gorongosa Mountain with its highest peak at 1836 metres above sea level (m a.s.l.) (The CGIAR Consortium for Spatial Information [CGIAR-CSI] 2008). Appendix 1 is a geological map over the Urema Rift and the area around GNP. Below is the geology of each morphological unit described in further detail.

2.2.2.1 The Báruè Platform

The surface of the Báruè Platform is gently sloping towards southeast until an abrupt decline at the rift margin (Tinley 1977). The Báruè Supergroup, which constitutes the major part of the platform and is the source of its name, is of Mesoproterozoic (1600-1000 Ma) age and consists of a metamorphic crystalline

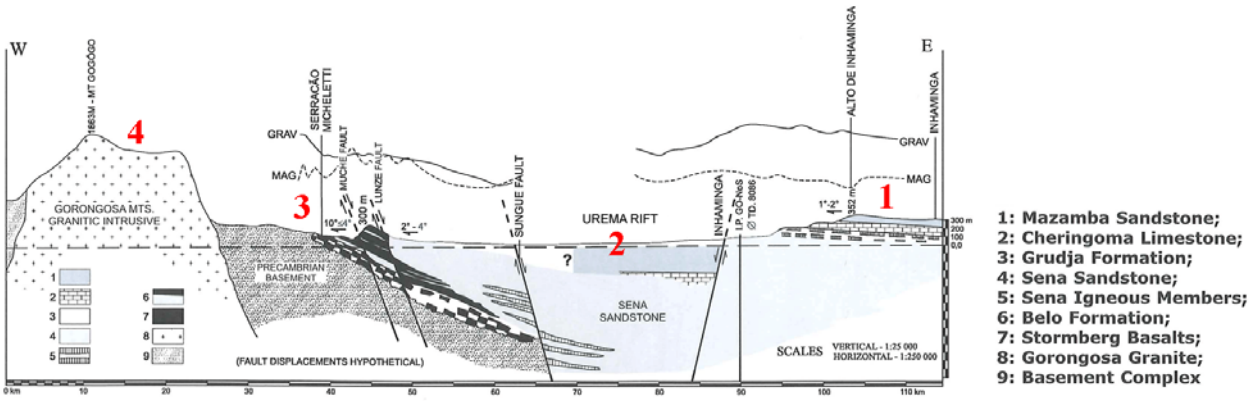

Fig. 3. Vertical geological cross-section of the Urema Rift, stretching from the Gorongosa Mountain to Inhaminga. The location of the transect is marked by the blue line in figure 2. The figure is modified from Lächelt (2004).

basement. The supergroup comprises five groups of granitic and migmatitic gneisses and feldspathic quartzite (Tinley 1977, National Directorate of Geology [DNG] 2006). North and south of the Gorongosa Mountain, swarms of granophyre and dolerite dykes has intruded the basement (Tinley 1977).

North and south of the Nhandugue River, east of Gorongosa Mountain, the Sena Formation and the Lupata Group is present. The Sena Formation formed during the lower Cretaceous in a continental setting. The formation consists of more or less massive conglomeratic arcosic sandstones, cemented with calcic-argillaceous material (Tinley 1977, Lächelt 2004, DNG 2006).

Lupata Group formed during the Post-Karoo Period and comprises red sandstones and phonolitic lava (Tinley 1977, Lächelt 2004, DNG 2006). The sandstones are divided into two formations, the Lower and Upper Lupata Formations (Lächelt 2004). The lower formation is 80-100 m thick and consists of a series of terrigenous conglomerates and sandstones (Lächelt 2004). Also the Upper Lupata Formation is composed of conglomerates and conglomeratic sandstones but also contains quartz-feldspar sandstones and fragments of the surrounding intrusive rocks (Tinley 1977, Lächelt 2004). Together with the upper formation the phonolitic lava forms a volcanosedimentary sequence (Lächelt 2004).

The Báruè Platform is mainly covered with poor sandy soils, weathered from the Báruè Supergroup. However, the mica associated with the Báruè Supergroup have produced layer-silicate clays such as montmorillonite and the intruding dolerite dykes breaks down into fertile red clayey latosols (Tinley 1977). The upper Lupata Formation, found south of the Nhandugue River, produces calcium-rich red clays and sandy clays, while the Sena Formation, north of the river, weather into sands and calcareous sandy clays (Tinley 1977).

2.2.2.2 The Gorongosa Mountain

The igneous complex consisting of granites and gabbros that now forms the Gorongosa Mountain intruded the Báruè Platform in the late Jurassic to early Cretaceous (Lächelt 2004, DNG 2006). Gabbros were first to intrude, and in the contact with the crystalline gneisses of the platform pyroxene and amphibolite hornfels were produced (Tinley 1977). The major part of the mountain consists of a micropegmatite granite pluton. When that intruded it also produced quartzitic hornfels on its contact with the crystalline gneisses (Tinley 1977).

The soils of the Gorongosa Mountain have mainly been produced by denudation and colluviation. Large deposits of colluvium are found on the northern and the south/southeastern slopes of the mountain (Tinley 1977, DNG 2006). The acid micropegmatite granite has produced mainly sandy ferralitic soils and humus-rich podsols, while the gabbros have been broken down into gritty ferromagnesoium-rich loamy clays (latosols) (Tinley 1977).

2.2.2.3 The Cheringoma Platform

The Cheringoma Platform on the eastern side of the rift valley consists of a cuesta, a seaward inclined block (Tinley 1977). The slopes facing the rift are steep, while the seaward slopes are gently sloping to the southeast. The cuesta consists of upper Cretaceous to recent sediments, but on the rift ward side of the block the slightly older Sena Formation is present (Tinley 1977).

The lowest part of the cuesta block is composed of the 200 m thick Grudja Formation mainly consisting of a marine sequence of yellowish-green glauconite sandstone. Interbedded in the sandstone are marls and limestone containing high amounts of fossiliferous arenaceous (Tinley 1977). Overlaying the Grudja Formation is the Cheringoma Formation, a white to pinkish calcareous limestone, formed during Eocene (Tinley 1977). The formation is ~70 m thick and contains a large amount of fossil foraminifera. The Cheringoma Formation continues into the Miocene Mazamba Formation, divided into a lower and an upper formation. The lower formation is ~130 m thick and consists of red and purplish sandstone (Tinley 1977). The upper Mazamba Formation, which is also called Inhaminga Sandstone, is a yellowish-grey medium to coarse arcosic sandstone with conglomerate horizons (Tinley 1977, DNG 2006).

The soils of the Cheringoma Platform have developed from eluviation and illuviation, while its rift ward slopes have been subject to erosive processes (Tinley 1977). Weathering of the Mazamba Formation has resulted in a lower unit of pallid sands and an upper unit of beige pinkish-yellow to orange or deep red siliceous sand. The lower unit is rich in iron oxides and has an impermeable layer of clay, while the upper unit is massive and compact (Tinley 1977).

2.2.2.4 The Rift valley floor

The Rift valley floor constitutes the lowest part of the park and around Lake Urema it is situated at approximately 26 m a.s.l. (CGIAR-CSI 2008). The sedimentary fill consists mainly of Quaternary alluvial sediments, resting on top of the Mazamba Formation which in turn overlies the Sena Formation (Fig. 3; Lächelt 2004, DNG 2006). Strong seasonal variations in climate and extent of flooding, together with discharge from rivers on the rift sides, have influenced the development of the soils on the Rift valley floor. In general coarse sediments, like gravel and sand, have formed alluvial fans on the sides while finer sediments have been deposited further out on the valley floor (Tinley 1977, Chirindja & Hellman 2009). Related to different ages of the eastern and western faults, the fans on the eastern side of the valley are younger than those on the western side. At the eastern side of the Rift valley floor widespread deposits of colluviums are present (DNG 2006).

2.3 Climate and hydrology

2.3.1 Climate

The Gorongosa National Park falls within Köppen's tropical savannah climate (Tinley 1977). The Gorongosa Mountain, situated outside the park boundary, is an exception with its warm temperate rainy climate (Tinley 1977). The major determinant of the climate, especially the rainfall, in this area is the Inter-Tropical Convergence Zone (ITCZ) and the El Nino Southern Oscillation (ENSO) (United Nations Environment Programme [UNEP] 2002). The park is located within the southeast trade wind belt, but is during the southern summer (November-April) close to the southern limit of the northeast monsoon. The average temperature is high (25-30° C) and heavy rain (100-450 mm) falls during the summer, referred to as the rainy or wet season (Owen 2004, Beilfuss *et al.* 2007). When the ITCZ moves northward during winter (May-September) a shift takes place in the South Indian Ocean anticyclone, which results in a dry season with lower temperatures (average temperature 20-25° C) and less rain (>50 mm) (Owen 2004, Beilfuss *et al.* 2007).

2.3.2 Water balance — precipitation and potential evapotranspiration

The annual amount of precipitation (P) varies between the different morphological units (Fig. 4). Highest amount of rain is falling on the Gorongosa Mountain where the topography is generating a rainy microclimate. In total the maximum P on the mountain is 2000 mm/yr. On the Báruè Platform and the Cheringoma Platform less rain fall and on an annual basis P is 800-1200 mm/yr and 1000-1400 mm/yr, respectively (Owen 2004). The Rift valley floor experiences the lowest amount of rainfall, ranging from 600-1000 mm/yr. Opposite to P the potential evapotranspiration

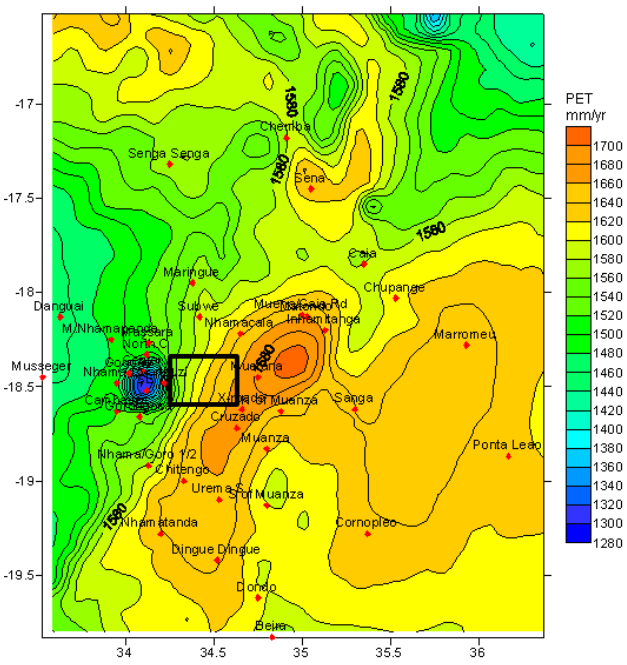

Fig. 5. Map showing values on annual potential evapotranspiration (PET) for the Southern African Sub Global Assessment (SAfMA) Gorongosa-Marromeu (GM) area. Highest PET values are concentrated to the Rift valley floor, while the lowest PET values are concentrated to the Gorongosa Mountain. The black rectangle marks the study area. The figure is adapted from Owen (2004).

(PET) is low on the mountain and high on the Rift valley floor, ranging from 1050-1650 mm/yr (Fig. 5; Owen 2004). Due to the strong seasonal variations in rainfall the major part of the park experiences a climatic water deficit during the dry seasons. It is only on the Gorongosa Mountain the annual water balance is positive. From here water drains trough perennial streams and probably much of the water is recharging

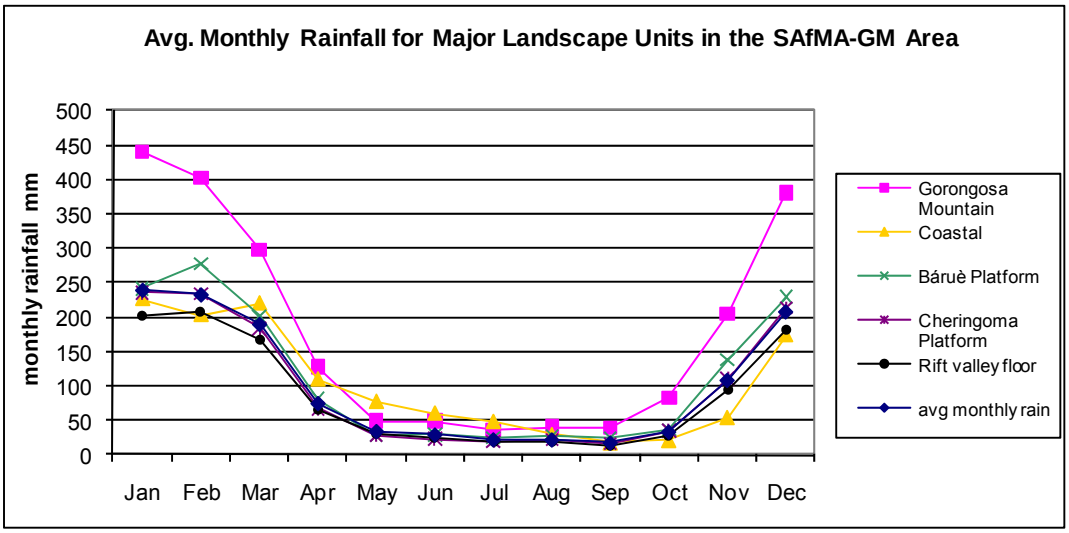

Fig. 4. Graph displaying average monthly rainfall in the different morphological units of the Southern African Sub Global Assessment (SAfMA) Gorongosa-Marromeu (GM) area. The graph is modified from Owen (2004).

groundwater storages along the rift margin. As long as the monthly P-PET water balance is positive the climatic water deficit does not automatically mean a lack of water in the ecosystem, and large parts of the Rift valley floor can remain wet during most, maybe even all, of the year.

2.3.3 The Urema Lake

The Nhandugue River, along which field work was conducted, is situated within the Urema Lake (Appendix 1) catchment area, which covers an area of 8755 km^2 (Böhme *et al.* 2006). The outlet of the lake is through the Urema River to the Pungwe River (Appendix 1), which then flows into the Indian Ocean. Due to annual variations in precipitation and evapotranspiration the naturally shallow Lake Urema is typified by large expansions and withdrawals of its shorelines. In high flood seasons the lake expands to cover more than 200 km^2, while during the dry seasons it recedes to between 12 and 15 km^2 in area (Böhme *et al.* 2006).

2.3.4 Effects of climate changes and land use

Consequences interpreted as due to global warming have been observed in the region and it has been anticipated that regional temperatures will rise, and thus increase the potential evapotranspiration (Moss *et al.* 2001). This will, even though the changes in precipitation have been simulated to be modest, increase the negative P-PET water balance, which will in turn constitute a threat on the water resources in the park. The effect of these climatic changes on the Urema Lake and associated floodplains needs to be understood and mitigated in order to effectively manage the water resources of the park.

Except for temperature and precipitation, several other factors affect the state of the Urema Lake. According to Chirindja & Hellman (2009) the lake is mainly fed by groundwater during dry seasons. This means the largest threats to the Urema Lake becoming desiccatated are structures which modify groundwater levels and create an increased gradient of subsurface drainage from the lake. Reintroduction of water-intensive cotton production and other irrigation projects may include extraction of groundwater and dams on seasonal and perennial rivers. Especially at the end of the dry seasons and during prolonged drought periods this will have a significant impact at some locations.

Around 250.000 people are living within the Urema Lake catchment area and of these ~15.000 are living in the park and ~25 000 just outside the park boundaries (GNP 2009). The slash-and-burn agriculture practised by the people affects the hydrology by reducing the total evapotranspiration, increasing the direct discharge and decreasing the groundwater recharge (Beilfuss *et al.* 2007). This has an especially important impact on the microclimate on the Gorongosa Mountain which is supporting the annual water flow into the Urema Rift. But if some of the surface discharge is captured as groundwater at the rift margin, and the Urema Lake is mainly fed by groundwater, then the effect of the land clearing may not be as severe (Beilfuss *et al.* 2007).

The Pungwe River is flowing along the southern park boundary, in the southeast joined by the Urema River. During the wet season the Pungwe is flooded and the water is inundating the wetlands south of the Urema Lake (Beilfuss *et al.* 2007). This flooding is vital for the wildlife sanctuary in the park and any changes in the natural discharge pattern by dams or water extraction from this river pose a significant threat to the GNP.

Not only changes in the hydrology are an effect of land use, but also the quality of the water may be affected. The ecosystem can only tolerate pollution and heavy minerals to a certain degree and to avoid toxic accumulation these limits of tolerance must be understood.

3 Study area

The Nhandugue River arises at the Great Escarpment on the border between Mozambique and Zimbabwe, and flows over the Báruè Platform just north of the Gorongosa Mountain. From the last outcrops of the crystalline basement the river flows in an incised river valley in the alluvial sands and then further onto the Rift Valley floor. Just before the Nhandugue River reaches the Rift valley floor, the Muche River (Appendix 1) is joining from the north. According to Tinley (1977), and confirmed during the field work, the Nhandugue River is a seasonal river. This means it has a surface flow that reaches Lake Urema only during the rainy seasons. Instead water might be flowing in the sediments from the rift margin and reach Lake Urema as groundwater.

Due to high discharge in the rainy seasons and low discharge in the dry seasons the river valley can be divided into three morphological units; (i) a dry-season channel (permanently filled with water), (ii) a wet-season channel (filled with water during rainy seasons) and, (iii) the river flanks (Fig. 6). The extent and location of these three units may show slight variations between different years, due to varying amount of discharge and changes in the route of the dry-season channel. Further, the river channel is becoming entirely dry during the dry seasons further towards Lake Urema, which was visually confirmed during the field work.

The field work was conducted during the dry-season, which made it possible to work on the river flanks, in the wet-season channel and also across the dry-season channel. Two areas, ~5 km apart from each other, were chosen. Area 2 is located approximately half a kilometre after the inflow of the Muche River into the Nhandugue River in the most eastern part of the Báruè Platform and Area 3 is located further downstream, on the Rift valley floor.

Fig. 6. Photo from Area 1, west of Area 2, showing the division of the Nhandugue River valley into three morphological units: (i) a dry-season channel (permanently filled with water), (ii) a wet-season channel (filled with water during rainy seasons) and, (iii) the river flanks. The width of the dry-season channel and wet-season channel is here approximately 200 m. The photo was taken in July 2010.

Fig. 7. Photos from Area 2 showing the dry-season channel and parts of the wet-season channel (left) and typical dense vegetation alternating with cultivated land in a part of the wet season channel (right). The photos were taken in July 2010.

Fig. 8. Photos showing side by side sections of the dry-season channel, the wet-season channel and parts of the river flanks from Area 3. The width of the dry-season channel and wet-season channel in the left photo is approximately 50 m. In the right photo the wet-season channel is approximately 100 m wide. The dense elephant grass present to the right in the left photo is same elephant grass present to the left in the right photo. The photos were taken in July 2010.

The soil cover in the selected Areas 2 and 3 is constituted to large extent of fine to coarse sands (Fig. 7-8). Finer material (silt and clay) is also present, mainly on the river flanks but also to some extent in the wet-season channel. Determined by field visits before the field work was started was that the vegetation cover is varying and at several locations very dense. The river flanks are entirely covered by alternating woody coverage, grass, bushes and cultivated land. Vegetation is also abundant in some parts of the wet-season channel. Especially in Area 2 the wet-season channel is to large extent covered by elephant grass, other types of grass, bushes, banana trees and cultivated land (Fig. 7). Breaking of the abundant vegetation is smaller open sand areas (Fig. 7). In Area 3 large parts of the wet-season channel are open sand areas, but parts covered with elephant grass, other types of grass, bushes and cultivated land also occur (Fig. 8).

4 Methods and materials

The methods used in this study was geophysical measurements (resistivity and induced polarisation), together with geological ground truthing and discharge measurements. Below all methods are described in further detail.

4.1 Geophysical surveying

4.1.1 Physical background and geological applicability

4.1.1.1 Resistivity

Resistivity (ρ) describes the ability of a material to be an isolator, i.e. the ability not to conduct an electric current. Depending on several factors different geological material have different resistivity. Igneous and metamorphic rocks have the highest resistivity values, which ranges from 1000 to 10^6 Ωm (Fig. 9; Loke 2004). The main factors affecting the resistivity for these types of rocks are the degree of fracturing and the percentage of fractures filled with water. Sedimentary rocks are often more porous and contains more water than the igneous and metamorphic rocks and have therefore lower resistivity values (10-1000 Ωm) (Fig. 9; Loke 2004). Unconsolidated sediments generally have even lower resistivity (from about 10 to >1000 Ωm), and the resistivity to great extent depend on porosity, degree of saturation and clay content (Fig. 9; Loke 2004).

To determine the resistivity for a geological material a controlled electrical current (I) is transmitted into the ground by two current electrodes and the potential (U) between two other electrodes (potential electrodes) is measured. By using Ohm's law (Equation 1) the resistance (R) can then be calculated (Dahlin 1993).

Equation 1:

$$R = \frac{U}{I}$$

R = resistance (Ω)
U = voltage in Volts (V)
I = current in Amperes (A)

From R the resistivity (ρ) can be derived in Ωm with Equation 2 by introducing a geometrical factor (K) (Reynolds 2007). This geometrical factor is depending on the electrode configuration, i.e. the arrangement of the electrodes and the distances between the individual electrodes.

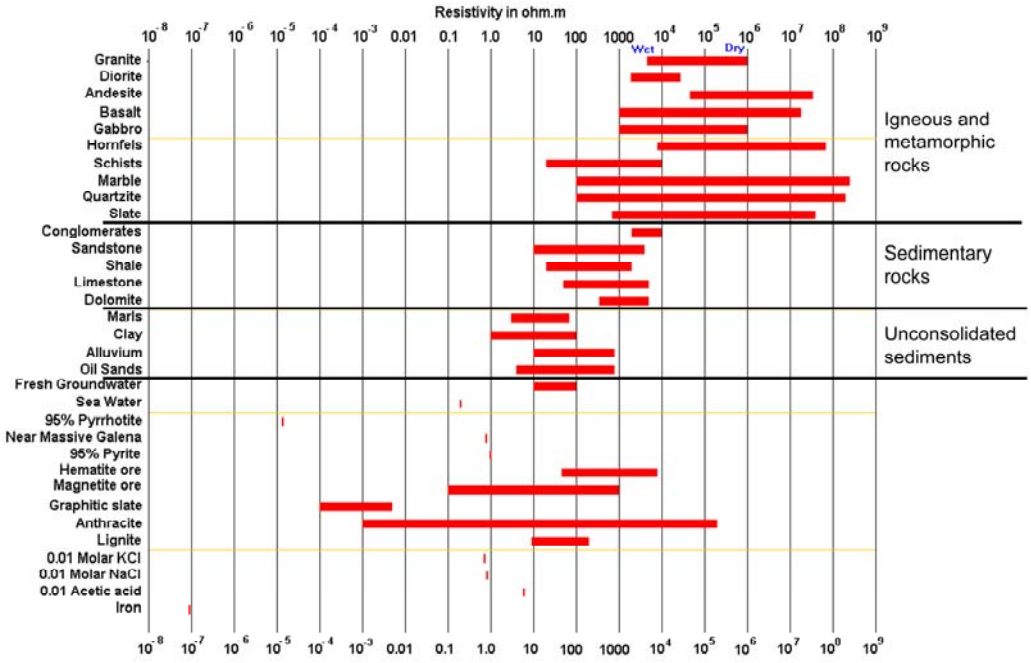

Fig. 9. Diagram displaying typical resistivity intervals for different materials, e.g. kinds of rocks, minerals and soils. The diagram is adapted from Loke (2004).

Equation 2:

$$\rho = K \times R$$

ρ = resistivity (Ωm)
K = geometrical factor
R = resistance (Ω)

Where the ground is not homogenous, which is almost always the case, the resistivity calculated is not the true resistivity, but the apparent resistivity (ρ_a) (Reynolds 2007). Measured in field is always the apparent resistivity, while estimates of true resistivities are obtained by data processing.

4.1.1.2 Induced polarisation

When a current is transmitted into the ground it will take some time for the potentials to reach a stationary value and also the potentials will not disappear immediately after the current is turned off (Dahlin 1993). Hence, the ground acts like a capacitor, which temporarily stores charge (becomes polarised) (Reynolds 2007). This phenomenon is known as IP-effect, where IP stands for induced polarisation. IP measurements can be useful complementary to resistivity measurements in cases where the resistivity model can be interpreted in alternative ways, due to broad and overlapping resistivity intervals (Jeppsson 2009). There are four different types of IP measurements available; time domain, frequency domain, phase domain and spectral IP. To combine measurements of resistivity and IP is usually not a problem as resistivity measurements are included in time-domain IP measurements.

With time-domain measurements the variation in voltage (U) with time is measured (Jeppsson 2009). This variation can be presented in mV/V or %, which is defined as chargeability (M). But most common is to present the results as apparent chargeability (M_a) in milliseconds (ms). The apparent chargeability is defined as the area under the decay curve of the overvoltage, arisen from switching of the current, between two times, t1 and t2 (Reynolds 2007).

4.1.2 Data collection

In total, resistivity and IP data were collected along six profiles, three within each area (Fig. 10). The locations of the profiles were chosen in order to get an as extensive data cover over the river valley sediments as possible. Hence, the river valley morphology, i.e. the extension of the dry-season and wet-season channels and the river flanks, together with the distribution of the soils and vegetation, which are further described in chapter 3 (Study area), were considered. For both areas a long profile was placed along the river channel, which was then crossed by two perpendicular profiles, stretching from the river flanks across the wet-season channel and the dry-season channel. To get measurements on where the profiles were located a GPS was used to mark the start- and endpoint of each profile, and every point along the profile where the instrument was measuring.

The method used for collection of data was 4-channel multi-electrode gradient array CVES roll-along measurements. For CVES (continuous vertical electrical soundings) measurements four multi-conductor cables are used. Every cable has 21 electrode takeouts at equal distances of either 2 or 5 metres, depending on wanted resolution and depth penetration (Jeppsson 2009). In this case an electrode spacing of 5 m was chosen, giving a depth penetration of

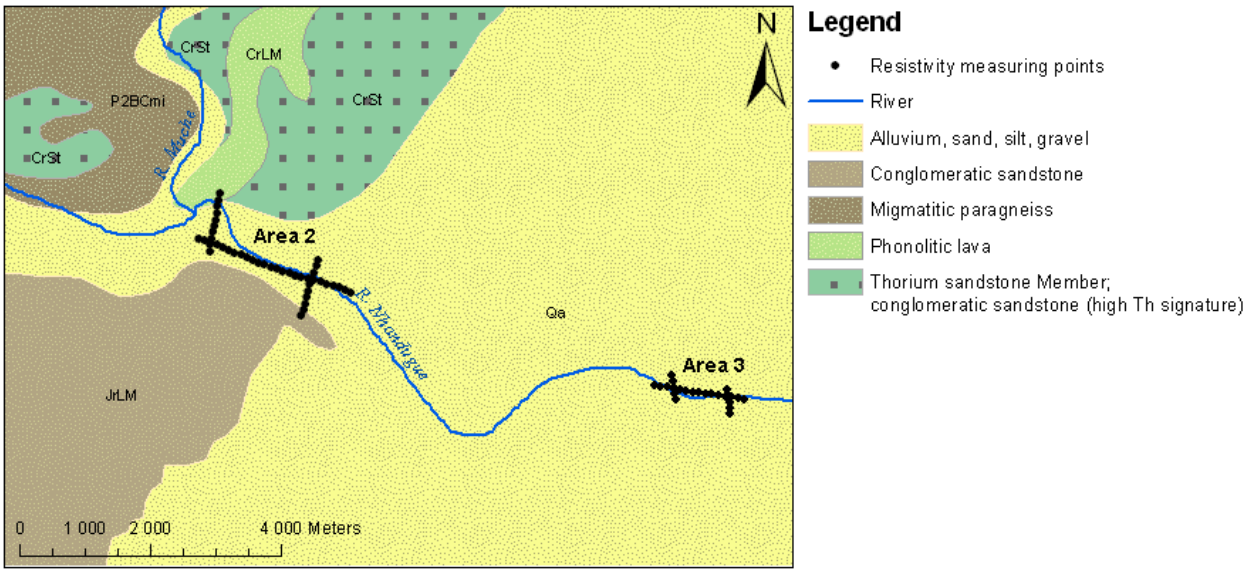

Fig. 10. Map showing locations of the measured resistivity profiles for Areas 2 and 3. Geologic units are transferred from the geological map (DNG 2006). The geological map has been mapped at the scale of 1:250 000, which means when zooming in to this extent there is a certain degree of inaccuracy in boundaries between different geological features. Due to natural variations in the position of the Nhandugue River with season and between the years, the map shows a mean position of the river. Therefore an inaccuracy occurs in the location of the resistivity profiles in relation to the river and the different geological features.

~60 m and the array a total length of 400 m. In order to measure continuous data for a longer distance than 400 m, so called roll-along measuring was applied. This means when all measurements on four cables are complete, the first cable of the array is moved to a new position after the fourth cable in the profile direction and new measurements are started (Fig. 11; Jeppsson, 2009).

The maximum depth penetration is depending on chosen electrode configuration, which in this case was a multiple gradient array. In a multiple gradient array a direct current (DC) is injected, in this case varying between 20 mA and 200 mA, with a separation of (*s*+2)a and simultaneously or sequentially picking up all the potential differences between electrodes with spacing a (Fig. 12; Dahlin & Zhou 2006). The separation factor (*s*) is here the maximum number of potential readings for a current injection, i.e. an integer. The smallest relative spacing between a potential electrode and a current electrode can be defined as the *n*-factor and the midpoint of the potential electrode dipole and the relative midpoint of the two current electrodes can be defined as a midpoint-factor, *m* (Dahlin & Zhou 2006). The *m*-factor can be negative or positive, depending on if the potential electrode dipole is situated to the left (negative) or to the right (positive) of the current electrode midpoint (Dahlin & Zhou 2006). Opposed to traditional gradient surveying, multiple gradient surveying uses a large number of current electrode combinations, scanning across the electrode array with several different spacings (*a*) and/or separations (*s*) (Dahlin & Zhou 2006). The larger the relative separation of current and potential electrode is, the deeper the depth penetration of the configuration.

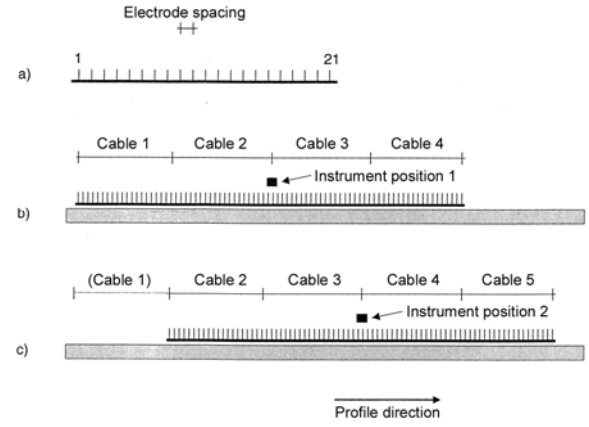

Fig. 11. Principle sketch of CVES resistivity roll-along measurements. The sketch is modified from Jeppsson (2009).

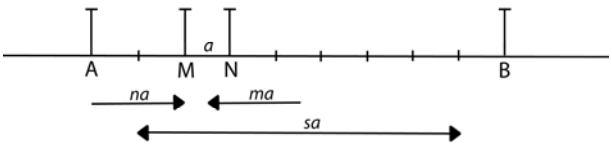

Fig. 12. Principle sketch showing electrode positions of a gradient array with a separation of (*s*+2)*a*, where the separation factor (*s*) = 7, the *n*-factor = 2 and the midpoint factor (*m*) = -2. The sketch is adapted from Dahlin & Zhou (2006).

The equipment used was an ABEM Terrameter SAS 4000, an ABEM LUND Resistivity Imaging System, an Electrode Selector ES10-64C, four multiconductor cables with 21 takeouts on each, cable-to electrode jumpers, a 12V DC battery and steel electrodes. To measure both IP and resistivity the terrameter was adjusted to IP mode. For logging of data in the instrument the two protocol files GRAD4LX8 and GRAD4S8 were used, since they are intended for 4-channel multiple gradient CVES with 4 electrode cables (ABEM 2009). First the long GRAD4LX8-protocol was measured, using an electrode spacing of 10 m, i.e. every other electrode. To improve the data cover for the largest depth the GRAD4LX8-protocol is supplemented with Wenner-Schlumberger measurements (i.e. another electrode configuration). When the long protocol was finished the short GRAD4S8-protocol was measured, using an electrode spacing of 5 m, in order to improve the near-surface data-cover (ABEM 2009)

4.1.3 Measurement and calculation of profile topographies

To get the topography along the resistivity profiles, elevation surveying was conducted. The materials used were two cm-graded sticks, a just over 20 m long string, a clinometer and a regular compass (360°). The string was attached to the sticks at fixed heights above ground, while the length was adjusted along the profile in order to reflect the surface morphology. The clinometer was attached on the string in the middle of the two sticks. An angle (in degrees) of the slope could then be read and noted together with the length of the string.

All data were put into an Excel-file and all angles in degrees were converted to radians. The height variation in relation to the previous measuring point could then be calculated according to equation 3.

Equation 3:

$$Height\ \ difference\ \ = a + (\sin(b) \times c)$$

a = previous height
b = angle in radians
c = distance from previous height measuring point

To get the height variation in m a.s.l. the elevation of the starting point was taken from a digital elevation model (CGIAR-CSI 2008) in ArcGIS 9 software. For the long profile in Area 2 the topography had to be corrected due to an excessive height difference from start to end. This correction was made by extracting a corrected height value (y_{end_corr}) for the

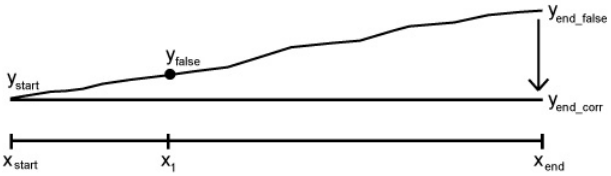

$$y_{corr} = y_{false} - \left(y_{end\_false} - y_{end\_corr} \times \frac{x_1 - x_{start}}{x_{end} - x_{start}}\right)$$

Fig. 13. Principles and equation for recalculation of excessive height values in metres above sea level (m a.s.l.). Values on y_{start}, y_{false}, y_{end_false}, x_{start}, x_1 and x_{end} are calculated from field data, while a corrected height value for the end-point y_{end_corr} is extracted from a digital elevation model.

end-point from the digital elevation model (CGIAR-CSI 2008) and then recalculation of false height values (y_{false}) for all points along the profile according to figure 13. The measured surface topography is shown in each profile in figure 15 and 21 and in Appendices 2 and 3

4.1.4 Data processing

In the field apparent resistivity and apparent chargeability were measured. Such data is usually presented in so called pseudosections, but in that format it can not be used as a base for geological interpretation since the values are not referring to a specific point, layer or unit (Jeppsson 2009). In order to obtain resistivity models displaying estimations of true resistivity values, computer processing of the data is needed. This process is called inversion and can be described with the following steps.

1. Measured data are displayed in a pseudosection.
2. A starting model is assumed.
3. The program calculates the pseudosection the assumed model would give rise to.
4. The measured pseudosection is then compared to the calculated section.
5. From the difference between the two pseudosections the model is adjusted.
6. A new pseudosection is calculated for the adjusted model and then steps 4 and 5 are repeated until the difference between the pseudosections is less than a prescribed number, e.g. 5 %. Then the iterations are stopped and the last model is adopted.

In order to process the measured data, softwares SAS4000 Utilities, RES2DINV ver.3.58.14 and Erigraph 2 were used. The data was first downloaded from the instrument and converted to DAT-format in the SAS4000 Utilities software from ABEM Instrument AB. The calculated topography values were then added to the DAT-file before it was opened in the RES2DINV software. In RES2DINV removal of bad data points and inversion (Robust inversion) with 3-7 iterations of the resistivity data was conducted. Final editing (depth interval, resistivity intervals, etc.) of the resistivity and IP models was made in Erigraph 2.

4.2 Geological ground truthing

For geological ground truthing surface soil samples, from a depth of ~15-30 cm, were collected at locations along the resistivity profiles (Fig. 14). In addition, three rock samples from an outcrop of Sena Formation and one soil sample from a gravel pit (G.P) north of the long resistivity profile in Area 2 were collected. The surface sampling was complemented with hand-held auger drilling at five sites along the profiles (Fig. 14). Table I shows the augering depth for each borehole. Samples were collected from borehole BH1-2, BH4 and BH6. In total 43 soil samples and three rock samples were collected from Area 2 and 3. The samples were to be analysed at Lund University, but due to transport costs only 33 of the soil samples and two pieces of the rock samples could be transported to Sweden. Representative surface samples from each profile were sent together with all borehole samples, two pieces of the rock samples and the soil from the gravel pit. To minimize the weight, only 500-600 g of each sample was taken. Performed analyses on the samples were grain size analyses (including sieving and hydrometer analysis), determination of loss on ignition (LOI), mineralogical composition and carbonate content. An overview of which analyses were performed on which samples is presented in table II.

4.2.1 Grain size analyses

4.2.1.1 Sieving

All samples were oven-dried at 105 ºC overnight. Then, depending on grain size and sorting, 200-500 g of each sample was used for sieving analyses. Each sample was put in a plastic bowl and dispersed with 0.05 M sodium pyrophosphate ($Na_4P_2O_7$) to dissolve all aggregates. To remove all grains smaller than 0.063 mm all samples were wet sieved through a sieve with a mesh size of 0.063 mm. The samples were collected in metallic bowls with a low water beam, then decanted and dried over night in 105 °C. After weighing each sample and bowl the samples were put in sieve stacks and placed in a sieve shaker for 15 minutes. The content in each sieve was then weighed.

4.2.1.2 Hydrometer analyses

Hydrometer analysis was conducted on all samples containing over 10 % grains smaller than 0.063 mm. The clay content was expected to be low and therefore approximately 100 g, or what was left after sieving, of each sample was used for the analysis. The oven-dried samples were pulverized and placed in a 1000 ml plastic measuring cylinder. 100 ml sodium pyrophosphate ($Na_4P_2O_7$) and 300 ml distilled water was added and the top of the cylinder was sealed with parafilm. The cylinders were rotated in a cradle for 15 minutes and the distilled water was added up to 990 ml. The

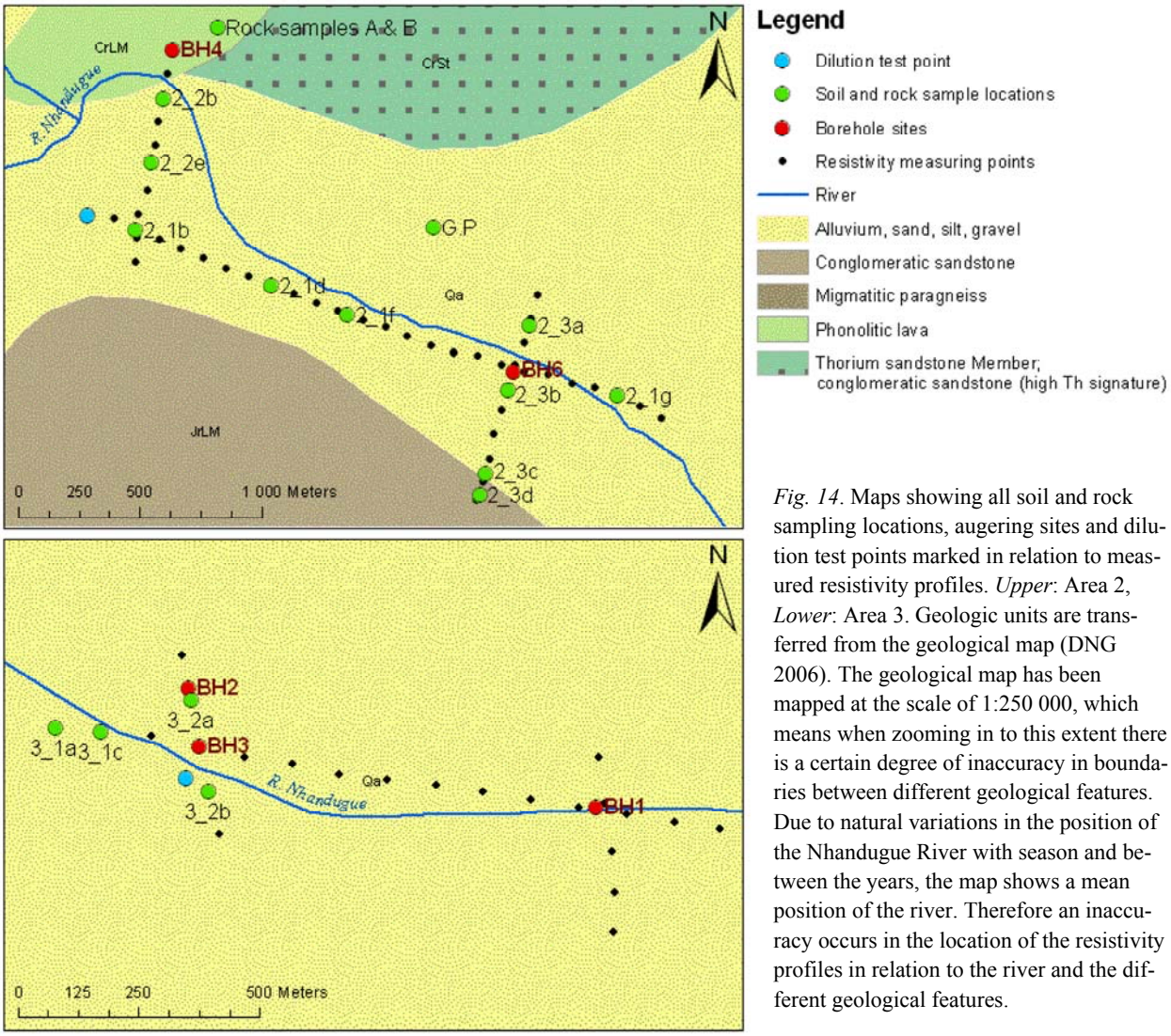

Fig. 14. Maps showing all soil and rock sampling locations, augering sites and dilution test points marked in relation to measured resistivity profiles. *Upper*: Area 2, *Lower*: Area 3. Geologic units are transferred from the geological map (DNG 2006). The geological map has been mapped at the scale of 1:250 000, which means when zooming in to this extent there is a certain degree of inaccuracy in boundaries between different geological features. Due to natural variations in the position of the Nhandugue River with season and between the years, the map shows a mean position of the river. Therefore an inaccuracy occurs in the location of the resistivity profiles in relation to the river and the different geological features.

Tab. I. Augering depths for borehole BH1-4 and BH6.

Borehole ID	Augering depth (m)
BH1	1.48
BH2	4.15
BH3	1.45
BH4	2.52
BH6	2.20

content was mixed for one minute with an agitator. When the agitator was taken out the time for the analyses was started. The agitator was washed with distilled water up to 1000 ml and a hydrometer was placed in the mixture. Readings were conducted at 30 seconds, 1, 2, 5, 10, 20, 50, 100, 200 and 400 minutes and 24h from the start. To get more reliable values the analysis of each sample was restarted after the last reading, and mean values were then calculated for the first 20 minutes.

4.2.1.3 Data processing

All data from the sieving and hydrometer analyses was put into the Excel-file KORNSTOR.xls. There grain size distribution in percentages and cumulative percentages were calculated and grain size distribution graphs were drawn. From the distribution graphs and calculated percentages grain sizes were determined according to guiding values in *Kompendium i jordartsanalys – laboratorieanvisningar* (Ambrosiani 1995).

4.2.2 Calculation of hydraulic conductivity

Hydraulic conductivity (K) was calculated with Hazen's formula (Equation 4), as defined by Chapuis (2004), for samples with a uniformity coefficient (C_u) <5. The uniformity coefficient describes the sorting of a material and is given by Equation 5 (Bowen 1986). Values for d_{60} and d_{10} were extracted from the grain size distributions graphs

Equation 4:

$$K = 0{,}0116 \times d_{10}^{\ 2}$$

K = hydraulic conductivity (m/s)
d_{10} = grain size that is 10% finer by weight

Tab. II. Chart over all soil and rock samples with performed analyses marked for each sample.

Sample	Sieving	Hydrometer	Loss on ignition	Carbonate content quick-test	Mineralogy
Area 2					
2_1b	X			X	X
2_1d			X	X	
2_1f	X		X	X	
2_1g	X	X	X	X	
2_2b			X	X	
2_2e	X	X	X	X	
2_3a	X	X	X	X	
2_3b	X			X	
2_3c	X			X	
2_3d	X			X	X
BH4a	X	X	X	X	
BH4b	X	X	X	X	X
BH4c	X	X	X	X	
BH4d	X	X		X	
BH4e	X	X		X	
BH4f	X			X	
BH4g	X	X		X	
BH4h	X			X	
BH6a	X	X		X	
BH6b	X	X		X	
BH6c	X			X	
BH6d	X			X	
BH6e	X			X	
G.P	X	X		X	X
Rock sample A				X	X
Rock sample B				X	X
Area 3					
3_1a	X			X	X
3_1c	X			X	
3_2a			X	X	
3_2b	X			X	
BH1a	X			X	
BH2a	X	X	X	X	
BH2b	X	X	X	X	
BH2c	X	X	X	X	
BH2d	X	X	X	X	

Equation 5:

$$C_u = \frac{d_{60}}{d_{10}}$$

d_{60} = grains size that is 60 % finer by weight
d_{10} = grain size that is 10 % finer by weight

4.2.3 Loss on ignition

Loss on ignition analyses (LOI) were conducted to determine the amount of organic matter in organic containing samples. Ceramic crucibles were oven-dried at 105 ºC overnight and cooled in a desiccator. Dried samples of 4-5 g were pulverized and placed in the crucibles and then oven-dried again at 105 ºC for one hour. The crucibles and samples were weighed on a balance with a three decimal accuracy and were then combusted for 2 h at 550 ºC. To prevent incomplete combustion the samples were placed in a cool oven and the temperature was slowly increased. After combustion the samples were cooled in a desiccator and then weighed. The weight difference between before and after combustion was then calculated and LOI was calculated in percentages by dividing the weight

difference with the weight of the dried sample, multiplied by 100.

4.2.4 Mineralogical composition

In order to attain an idea of the origin of the fluvial deposits in the river valley the mineralogical composition of five soil samples were optically analysed. Grains chosen for this analysis had a diameter of 2 mm. A light microscope was used and the grains were divided into pure quartz, other crystalline, sandstone, volcanic and secondary concretions. In total ~300 grains were counted in each sample. The number of grains in each group was counted and percentages were calculated.

The two pieces of rock samples were optically studied with a light microscope and classified according to Tucker (2001) (Fig. 15). The intact samples were studied and, due to the poor consolidation, a piece of each sample was also pulverized and studied.

4.2.5 Carbonate content

The Sena Formation sandstone has been classified as arcosic sandstone cemented with calcic-argillaceous material. In order to complement the mineralogical composition study and to decide if a part of or all the material in the soil samples originates from the sandstone the amount of calcium carbonate (CaCO3) in both the sandstone and soil samples was estimated with a quick-test with hydrochloric acid. Approximately 2 g of soil was moistened with some water in a ceramic bowl. For the rock samples a small piece of the sample was pulverized by hand and moistened. A few drops of hydrochloric acid (10 % solution) were then added and the amount of CaCO3 was determined from the magnitude of milling according to table III.

4.3 Discharge measurements (dilution tests)

To estimate the downstream change in surface discharge (Q) dilution tests were conducted. A dilution test is a tracer method, which is based on measurements of the passage of an upstream injected known amount of a tracer substance (Benischke & Harum 1990). Test were conducted at two locations, one in Area 2 and one in Area 3 (Fig. 14). In order to get reliable data sections where the river flowed in one single were chosen. For the tests 500 g of normal table salt (mainly NaCl) was dissolved in 20 L of water and the electrical conductivity (*EC*) of the solution was measured using an HQ40d Dual-Input Multi-parameter Meter Configurator. By using "*EC*-masses" ($M \times EC_1$) instead of NaCl-masses it was avoided to have to dry and weigh the salt and to determine the specific relationship between salt and electrical conductivity, (Merkel & Steinbruch 2008). The solution was poured into the water stream in a way that it would be well mixed with the water. At the same time continuous measurements (approximately every second) of the *EC* was started 10 m downstream of the injection point. Reading of data was conducted until the conductivity value was stabilized. *Q* was then calculated in L/s by equation 6, modified from Merkel & Steinbruch (2008).

Tab. III. Chart of approximate amounts of calcium carbonate ($CaCO_3$) in relation to the amount of carbon dioxide development. The chart is translated from Ambrosiani (1995).

Approximate amount of $CaCO_3$	Milling (Carbon dioxide development)
0.5% or less	None
0.5-1%	Extremely weak
1-3%	Weak
3-5%	Strong, but not sustained
> 5%	Strong and sustained

Equation 6:

$$Q = \frac{M \times EC_1}{\int EC}$$

EC = electrical conductivity in µS/cm downstream of injection point
M = the amount of water used (L)
EC_1 = electrical conductivity of the tracer solution

5 Results

5.1 Area 2

5.1.1 Geophysical surveying

The profiles from Area 2 all have a depth penetration of ~60-70 m. The long profile has a length of 2500 m, while the two cross-profiles are both 900 m long. The upstream cross profile (2_2) crosses the long profile at 200 m, while the downstream cross profile (2_3) crosses at ~1850 m.

5.1.1.1 Resistivity

A three-dimensional resistivity model over Area 2 is shown in figure 15. Two-dimensional resistivity models of the three profiles with layers outlined in black are displayed in Appendix 2 (A-C). The resistivity is in general highest at the surface and decreases with depth.

In the long profile, several small vertical heterogeneities are visible and four horizontal layers can be identified (Fig. 15, Appendix 2A):

- A topmost continuous high resistivity (330-1400 Ωm) layer of 5-10 m thickness.
- A ~5 m thick discontinuous layer of low to medium resistivity (8.8-37 Ωm)
- A medium resistivity (18-160 Ωm) layer which thickens, from ~10 to 30-40 m, in downstream direction.
- A bottommost low resistivity (1-18 Ωm) layer which becomes thinner, from ~40 to ~15 m, in downstream direction.

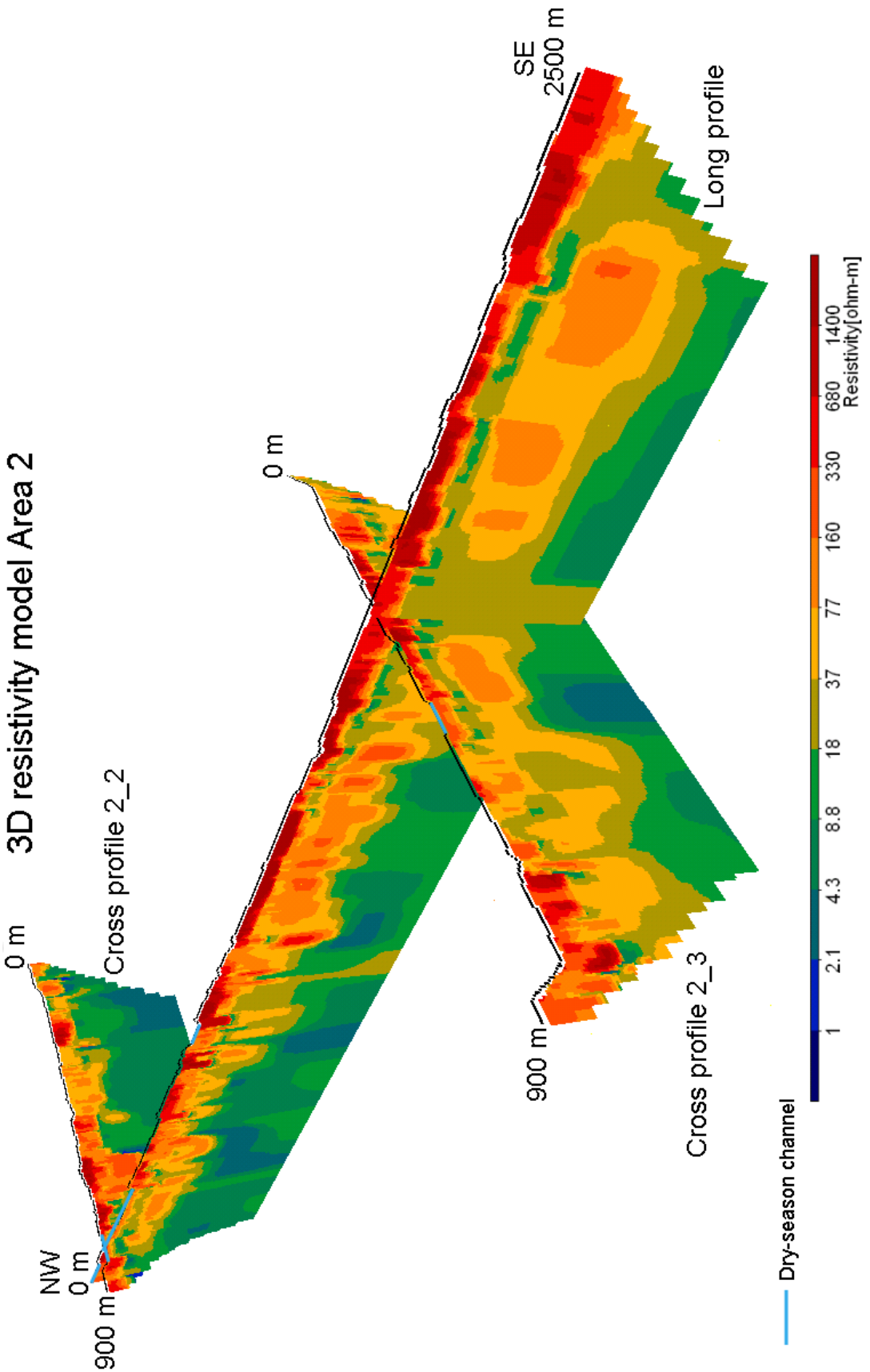

Fig. 15. Three-dimensional resistivity model for Area 2 including the long profile and the upstream and downstream cross profiles 2_2 and 2_3. Four different layers can be distinguished. The black line at the top of the sections represents the levelled ground surface.

The mean residual for the long profile is 7.1 % after seven iterations.

For the upstream cross profile (2_2), two main horizontal layers can be identified in the resistivity model (Fig. 15, Appendix 2B):

- A top layer with medium to high resistivities (37-1400 Ωm) and a varying thickness between 10 and 30 m.
- An underlying low resistivity (1-18 Ωm) layer of 45-65 m thickness.

In the SSW end of the profile and at midpoints 300 m and 500 m thin low resistivity (1-37 Ωm) lenses and a underlying medium resistivity (18-330 Ωm) layer of 10-15 m thickness can also be identified. The mean residual after three iterations is 5.8 %.

In the resistivity model for the downstream cross profile 2_3, four horizontal layers can be identified (Fig. 15, Appendix 2C):

- A topmost continuous high resistivity (330-1400 Ωm) layer of 10-15 m thickness.
- A discontinuous and thin low to medium resistivity (8.8-37 Ωm) layer of ~5-10 m thickness.
- A medium resistivity (18-160 Ωm) layer of 20-30 m.
- A bottommost low resistivity (1-18 Ωm) layer of about 30 m thickness.

The mean residual for the downstream cross profile 2_3 is 5.2 % after six iterations .

5.1.1.2 Induced polarisation

The results from the IP measurements show very high percentages of error. The mean residual is 45.1 % for the long profile after seven iterations, 37.5 % for the upstream cross profile (3_2) after three iterations and 22.0 % for the downstream cross profile (3_3) after six iterations (Appendix 3 A-C). These high error percentages indicate the profiles are not usable as a base for interpretations.

5.1.2 Geological ground truthing

All results from the grain size analyses, hydraulic conductivity calculations, loss on ignition and carbonate content analyses are presented in table IV. In figure 17 an overview of sample locations and types of

Tab. IV. Chart showing all samples from Area 2 and their respective grain size/type of soil, hydraulic conductivity, loss on ignition and approximate amount of $CaCO_3$.

Sample	Grain size/type of soil	Sand fraction for sand samples	Hydraulic conductivity (m/s)	Organic content (%)	Approximate amount of $CaCO_3$ (%)
2_1b	Gravelly sand		$1.85x10^{-3}$		≤0.5
2_1d	Mineral soil with organic matter			11.4	≤0.5
2_1f	Sand	Medium	$0.61x10^{-3}$	0.3	≤0.5
2_1g	Silty sand			3.0	≤0.5
2_2b	Mineral soil with organic matter			10.7	≤0.5
2_2e	Sand	Fine		1.7	≤0.5
2_3a	Clayey silty sand			3.3	≤0.5
2_3b	Sand	Medium	$0.38x10^{-3}$		≤0.5
2_3c	Sandy gravel		$2.45x10^{-3}$		≤0.5
2_3d	Sand	Medium-coarse	$0.38x10^{-3}$		≤0.5
G.P	Clayey gravelly sand				≤0.5
Rock sample A					≤0.5
Rock sample B					≤0.5
BH4a	Silty clayey sand			3.8	≤0.5
BH4b	Silty clayey sand			3.2	≤0.5
BH4c	Silty clayey sand			3.4	≤0.5
BH4d	Silty clayey sand				≤0.5
BH4e	Silty sand				≤0.5
BH4f	Sand	Medium-coarse			≤0.5
BH4g	Clayey sand				≤0.5
BH4h	Silty gravelly sand				≤0.5
BH6a	Clayey silty sand				≤0.5
BH6b	Partly silty clayey sand				≤0.5
BH6c	Partly silty sand		$0.22x10^{-3}$		≤0.5
BH6d	Sand	Medium-coarse	$0.41x10^{-3}$		≤0.5
BH6e	Partly silty sand		$0.30\ x10^{-3}$		≤0.5

soils/grain sizes are presented. All but three surface samples are classified as sand. Sample 2_1f, 2_2e, 2_3b and 2_3d consists of pure sand and are further classified into fine, medium and coarse sand. The remaining sand samples are further classified by the supplementary adjectives gravelly, silty and/or clayey. Of the three non-sand samples, sample 2_3 is classified as sandy gravel and samples 2_1d and 2_2b as mineral soil with organic matter. The amount of organic matter for these two samples is 11.4 % and 10.7 %, respectively.

According to table IV and the log in figure 18 the topmost layer (0-0.35 m) of borehole BH4 is classified as mineral soil with organic matter, while the main part of the borehole (0.35-2.50 m) consists of sand with varying silt, clay and gravel content. The colours of the different layers are varying between pale brown, dark brown and brown-reddish. From 0.35 m down to 1.95 m, larger angular particles and bedrock fragments are present. In the underlying layer (1.95-2.10 m) the larger particles (~2 cm) are rounded and larger pieces of pegmatite, quartz and iron oxide are present. Charcoal and iron oxides are present in the bottommost silty gravelly sand layer.

For borehole BH6 the first 0.75 m consists of mineral soil with organic matter (Fig. 18). The remaining part of the borehole (0.75-2.2 m) consists of fine-medium to medium-coarse sand (Tab. IV, Fig. 18). The second and sixth layer from the top layer consists of pure sand, while the other layers contain various amounts of silt and clay. The colours are varying from dark brown and pale brown to pale orange. Layer four from the top is homogenous and contains no large particles, while larger rounded particles are present in the underlying layer five.

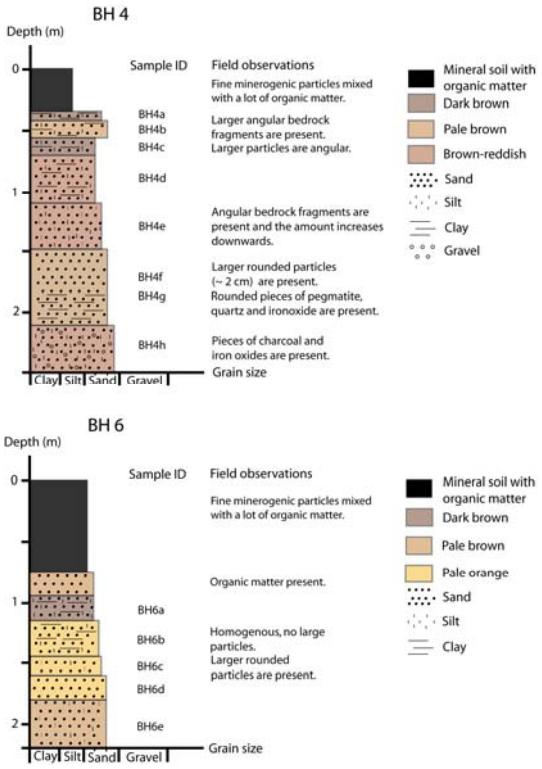

Fig. 18. Logs for borehole BH4 and BH6 in Area 2, showing types of soils, grain sizes, location of soil samples and field observations throughout the boreholes.

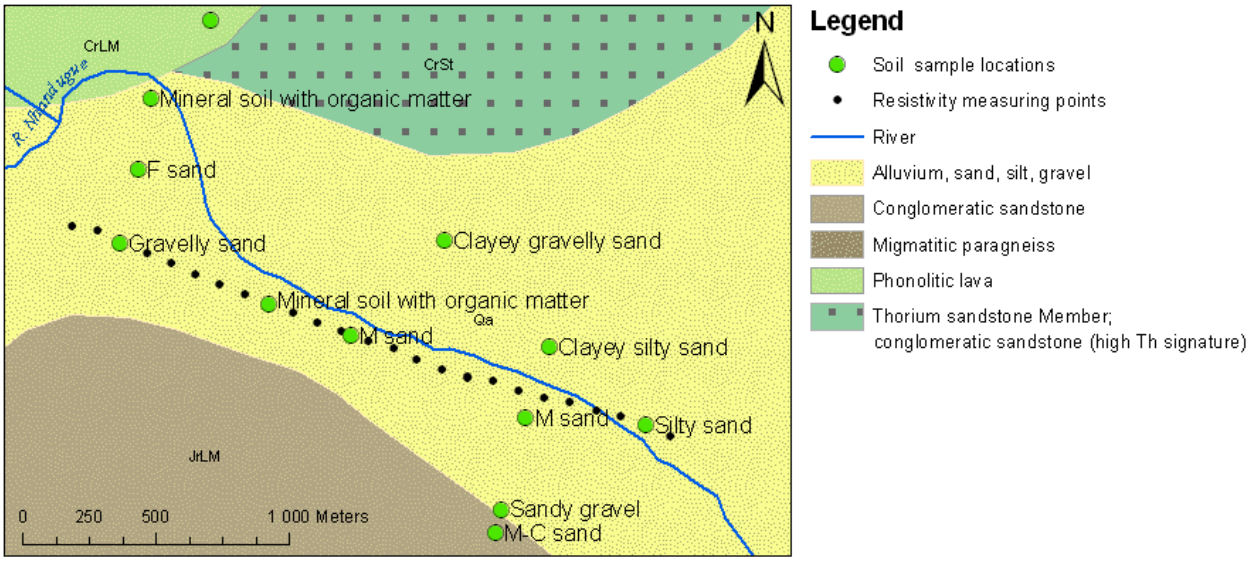

Fig. 17. Map showing location of different grain sizes and soil types in Area 2. Geologic units are transferred from the geological map (DNG 2006). The geological map has been mapped at the scale of 1:250 000, which means when zooming in to this extent there is a certain degree of inaccuracy in boundaries between different geological features. Due to natural variations in the position of the Nhandugue River with season and between the years, the map shows a mean position of the river. Therefore an inaccuracy occurs in the location of the resistivity profiles in relation to the river and the different geological features.

The hydraulic conductivity ranges from $0.22x10^{-3}$ m/s to $2.45x10^{-3}$ m/s (Tab. IV). The highest value is for sandy gravel (sample 2_3c), while the partly silty sand of sample BH6c has the lowest value. The amount of carbonate (CaCO3) is ≤0.5 % for all samples, including the rock samples (Tab. IV).

Analyses of mineralogical composition (Fig. 19) show that all four analysed samples are dominated by crystalline fragments (52.4-83.5 %). The second largest group is pure quartz, constituting 11.3-42.3 % of all grains. A few percentages (1.9-5.2 %) of sandstone fragments are present in all samples. Secondary concretions are present in sample 2_3d and the gravel pit sample, and 1 % volcanic fragments are present in 2_3d.

The mineralogical study of the rock samples shows Rock sample A to be massive, homogenous and fine grained (grains are in the sand fraction), while Rock sample B is conglomeratic and consists of grains of varying size in the sand to gravel fraction (Tab. V). They are both poorly consolidated and contains <15 % matrix. They consist of much quartz, but also feldspar, dark minerals and iron oxides. A white precipitation is visible in both samples. (Tab. V). Both pieces are classified as feldspar rich sandstone.

5.1.3 Discharge measurement (dilution test)

Measured values f electrical conductivity (EC) downstream of the injection point are presented as µs/cm over time (s) in figure 20. The integral for the measured *EC*-values was calculated to 2889 s·µS/cm, the *EC* of the tracer solution used was 30 900 µS/cm and the background *EC*-value for the river was 108.8 µS/cm. Calculations with equation 6 gave a discharge of 214 L/s on the 14th of August 2009.

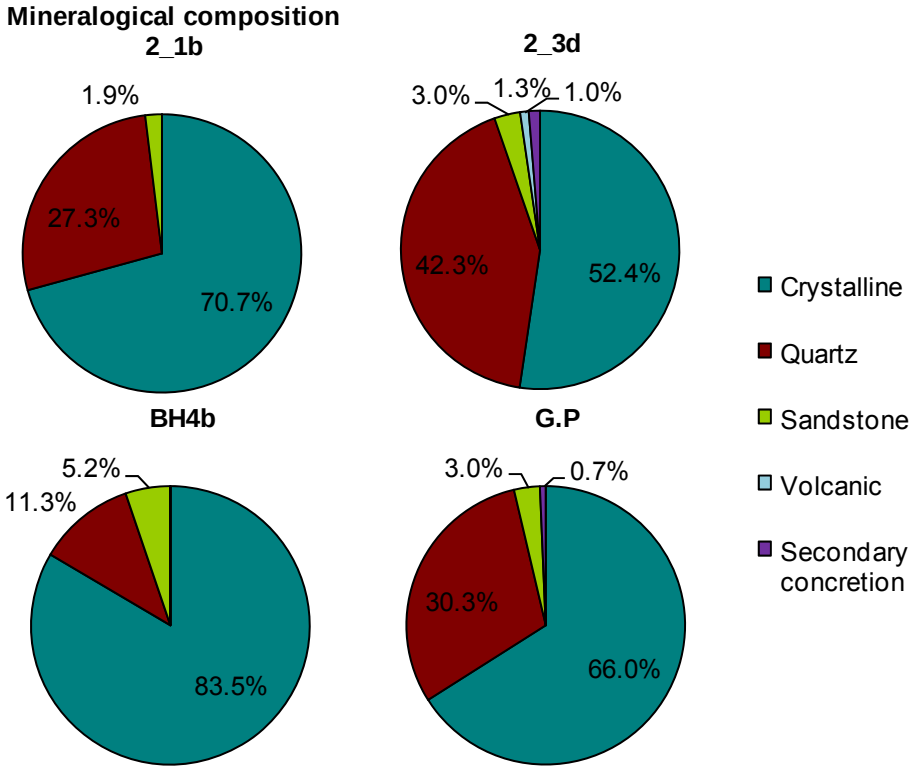

Fig. 19. Pie charts displaying the mineralogical composition for sample 2_1b, 2_3d, BH4b and G.P in percentages of total amount of counted grains.

Tab. V. Chart over observations and classification for rock sample A and B.

Sample ID	Observations	Classification
Rock sample A	Massive, homogenous and fine grained (sand fraction). Consists of much quartz. Contains feldspar, dark minerals and iron oxides. Poorly consolidated, low matrix content, white precipitations.	Feldspar rich sandstone
Rock sample B	Conglomeratic with grains of varying size (sand-gravel fraction). Consists of much quartz. Contains feldspar, dark minerals and iron oxides. Poorly consolidated, low matrix content, white precipitations.	Feldspar rich sandstone

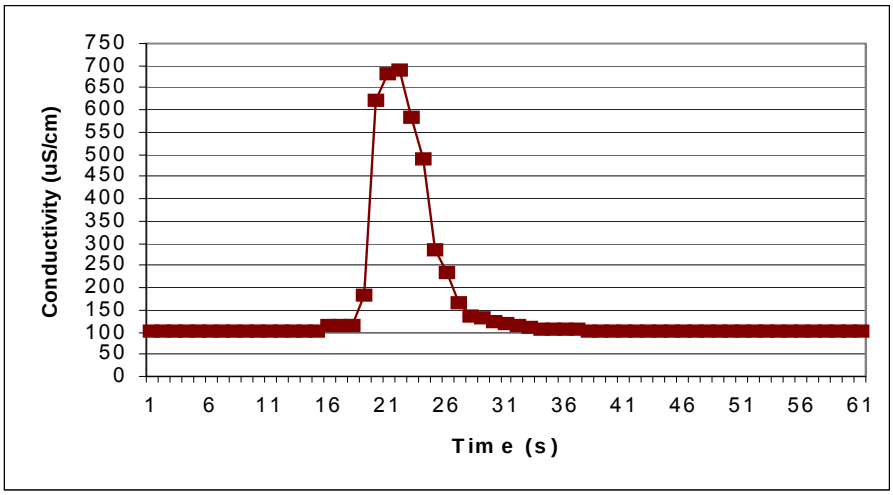

Fig. 20. Graph showing the relation between conductivity in µS/cm and time in seconds (s) for the dry-season channel in Area 2.

5.2 Area 3

5.2.1 Geophysical surveying

The profiles from Area 3 all have a depth penetration of ~60-70 m. The long profile has a length of 1400 m, while the two cross-profiles are both 400 m long. The upstream cross profile (3_2) crosses the long profile at 300 m, while the downstream cross profile (3_3) crosses at ~1150 m.

5.2.1.1 Resistivity

A three-dimensional resistivity model over Area 3 is shown in figure 21. Two-dimensional resistivity models of the three profiles with layers outlined in black are displayed in Appendix 2 (D-F). The resistivity is in general highest at the surface and decreases with depth.

In the resistivity model for the long profile three horizontal layers can be identified and a fourth underlying layer is indicated at the bottom (Fig. 21, Appendix 2D);

- A topmost continuous medium to high resistivity (37-1400 Ωm) layer of 5-8 m thickness.
- A low somewhat discontinuous resistivity (1-18 Ωm) layer of 5-8 m thickness.
- A low to medium resistivity (4.3-77 Ωm) layer of ~50 m thickness.

The mean residual for the long profile is 15.7 % after seven iterations.

For the upstream cross profile (3_2) three horizontal layers can be identified in the resistivity model and a fourth underlying layer is indicated at the bottom (Fig. 21, Appendix 2E);

- A 5-10 m thick top layer with medium to high resistivity (37-1400 Ωm).
- A somewhat discontinuous layer with low resistivity (1-18 Ωm) of ~10 m thickness.
- A low to medium resistivity layer (2.1-77 Ωm) of ~45 m thickness.

The mean residual for the upstream cross profile 3_2 is 10.9 % after seven iterations.

In the resistivity model for the downstream cross profile 3_3 three horizontal layers can be identified and a fourth underlying layer is indicated at the bottom (Fig. 21, Appendix 2F);

- A ~5-10 m thick topmost medium to high resistivity (37-1400 Ωm) layer.
- A low somewhat discontinuous resistivity (1-18 Ωm) layer of ~5-7 m thickness.
- A 45-50 m thick low to medium resistivity (4.3-37 Ωm) layer.

The mean residual for the downstream cross profile 3_3 is 7.3 % after seven iterations .

5.2.1.2 Induced polarisation

The results from the IP measurements show very high percentages of error. The mean residual is 157.6 % after seven iterations for the long profile, 403.7 % for the upstream cross profile (3_2) and 22.8 % for the downstream cross profile (3_3) (Appendix 3 D-F). These high error percentages indicate the profiles are not usable as a base for interpretation.

5.2.2 Geological ground truthing

All results from the grain size analyses, hydraulic conductivity calculations, loss on ignition and carbonate content analyses are presented in table VI. In figure 22 an overview of sample locations and types of soils/grain sizes are presented. Three of the four surface samples (3_1a, 3_1c and 3_2b) consist of pure sand, and they are further classified into medium and coarse sand. The remaining surface sample, 3_2a, contains 6 % organic matter and is classified as mineral soil with organic matter.

The log for borehole BH1 (Fig. 23) shows the entire borehole consists of pale brown sand. From the top and downwards the grain size changes from coarse to medium sand. In layer two from the top and in the bottommost layer, larger particles (~0.5-1 cm) are present. Borehole BH2 consists of medium to coarse pale brown sand (Tab. VI, Fig. 23). In varying amount larger particles (~ 0.5 cm) are present. For borehole BH3 the main part (4 m) consists of partly silty clayey sand (Tab. VI, Fig. 23). The colour is varying between

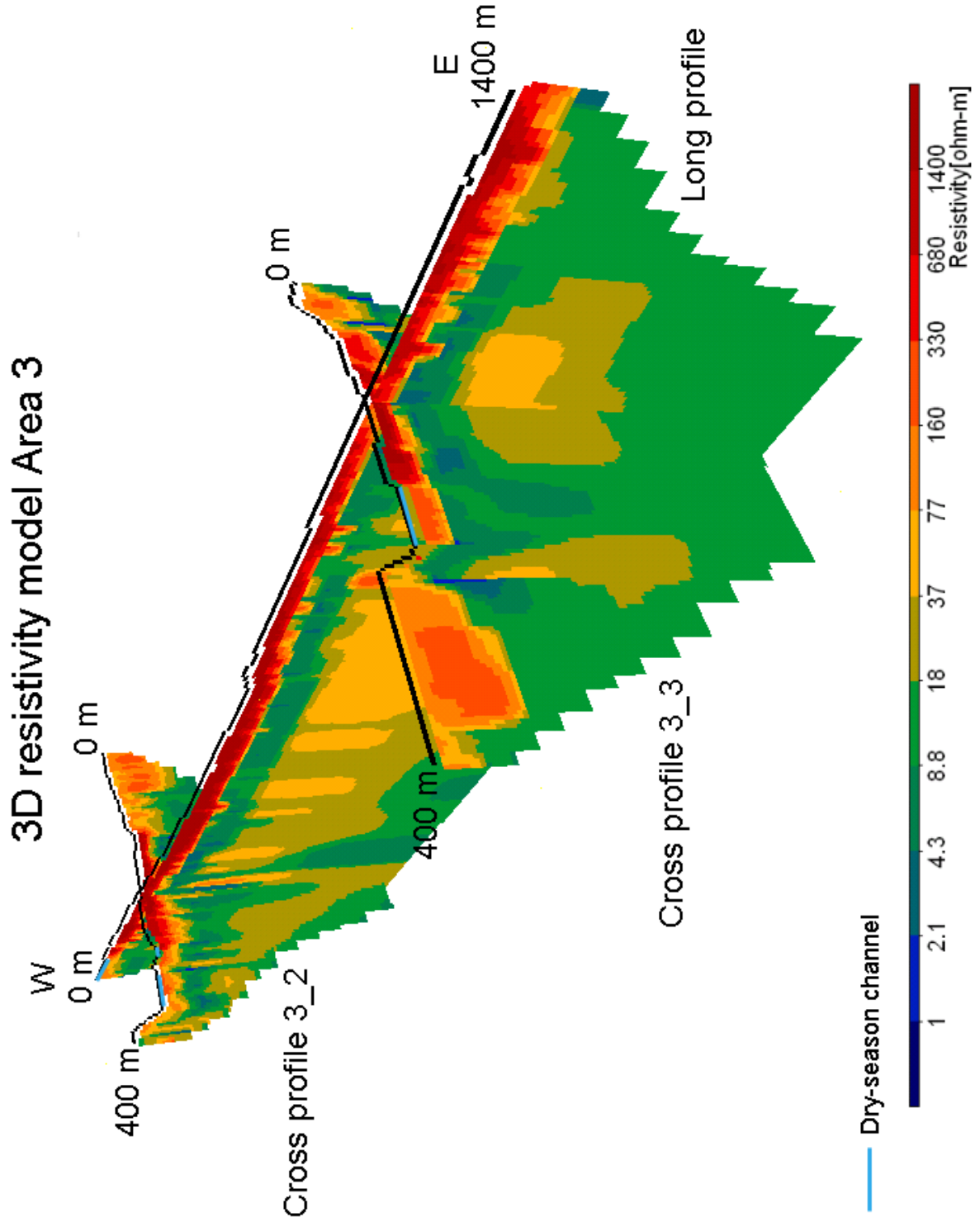

Fig. 21. Three-dimensional resistivity model for Area 3 including the long profile and the upstream and downstream cross profiles 3_2 and 3_3. Three different layers can be identified and a fourth underlying layer is indicated in the bottom. The black line at the top of the sections represents the levelled ground surface.

Tab. VI. Chart showing all samples from Area 3 and their respective grain size/type of soil, hydraulic conductivity, loss on ignition and approximate amount of $CaCO_3$.

Sample	Grain size/type of soil	Sand fraction for sand samples	Hydraulic conductivity (m/s)	Loss on ignition (%)	Approximate amount of $CaCO_3$ (%)
3_1a	Sand	Coarse	$1.18x10^{-3}$		0.5 or less
3_1c	Sand	Medium to coarse	$0.46x10^{-3}$		0.5 or less
3_2a	Mineral soil with organic matter			6.0	0.5 or less
3_2b	Sand	Medium	$0.72x10^{-3}$		0.5 or less
BH1a	Sand	Medium	$0.67x10^{-3}$		0.5 or less
BH2a	Partly silty clayey sand			2.8	0.5 or less
BH2b	Partly silty clayey sand			1.6	0.5 or less
BH2c	Partly silty clayey sand			2.1	0.5 or less
BH2d	Silty clayey sand			2.7	0.5 or less

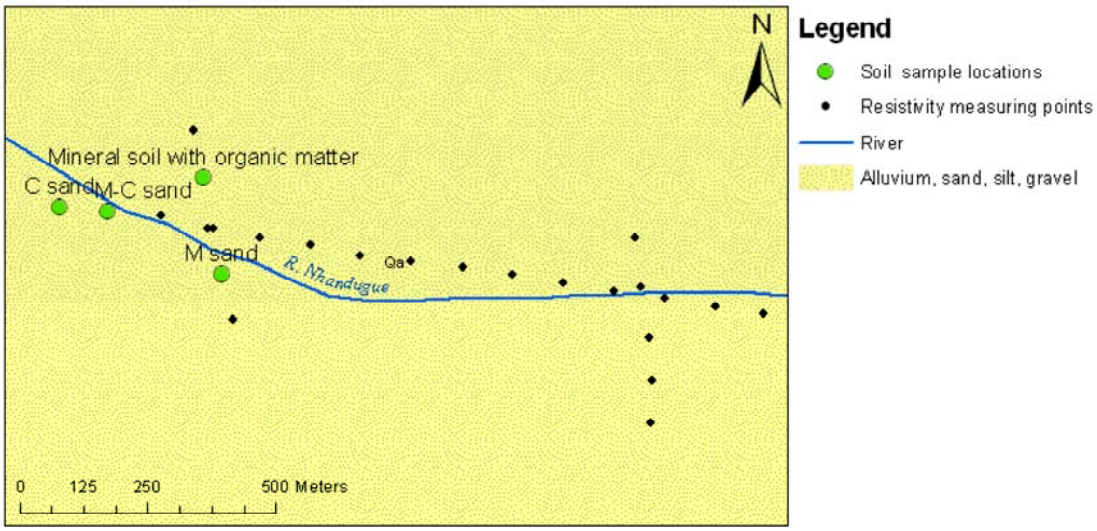

Fig. 22. Map showing location of different grain sizes and soil types in Area 3. Geologic units are transferred from the geological map (DNG 2006). The geological map has been mapped at the scale of 1:250 000, which means when zooming in to this extent there is a certain degree of inaccuracy in boundaries between different geological features. Due to natural variations in the position of the Nhandugue River with season and between the years, the map shows a mean position of the river. Therefore an inaccuracy occurs in the location of the resistivity profiles in relation to the river and the different geological features.

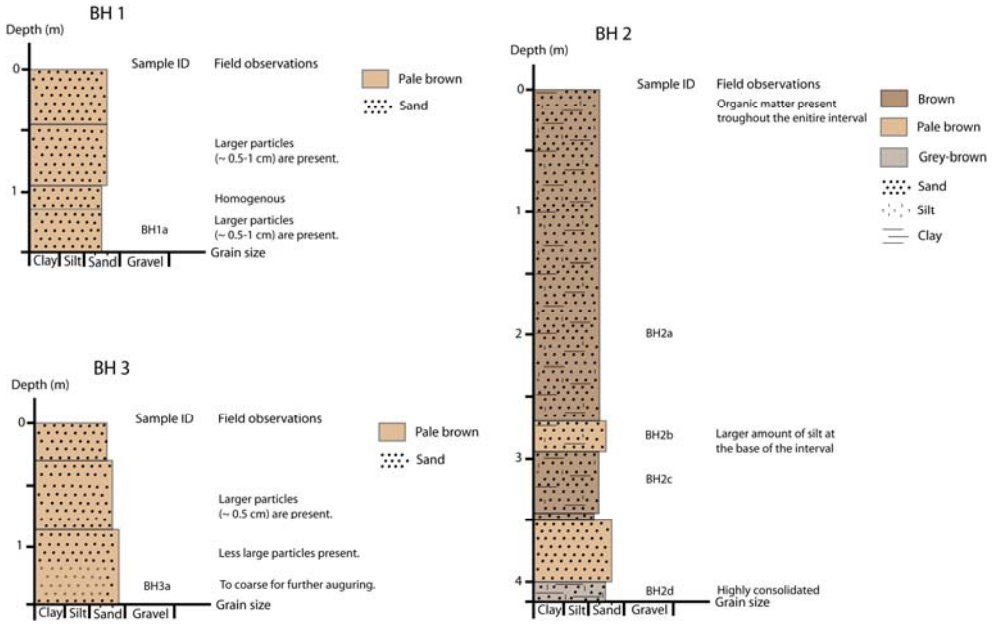

Fig. 23. Logs for borehole BH1-3 in Area 3, showing types of soils, grain sizes, location of soil samples and field observations throughout the boreholes.

brown and pale brown. At the bottom a grey-brown layer of much consolidated silty clayey sand is present.

The hydraulic conductivity ranges from $0.46x10^{-3}$ m/s to $1.18x10^{-3}$ m/s (Tab. VI). The highest value is for coarse sand (sample 3_1a), while the medium-coarse sand (sample 3_1c) has the lowest value. The amount of carbonate (CaCO3) is ≤0.5 % in all samples (Tab. VI). From the mineralogical analysis of sample 3_1a it is concluded the sample consists of 64.6 % crystalline fragments, 33.2 % pure quartz, 1.9 % sandstone fragments and 0.3 % volcanic fragments (Fig. 24).

5.2.3 Discharge measurement (dilution test)

Measured values of electrical conductivity (*EC*) downstream of the injection point are presented as µs/cm over time (s) (Fig. 25). The integral for the measured EC-values was calculated to 7824 s·µS/cm, the *EC* of the tracer solution used was 28 800 µS/cm and the background *EC*-value for the river was 105 µS/cm. Calculations with equation 6 gave a discharge of 74 L/s on the 14th of August 2009.

6 Discussions

6.1 Area 2

The grain size analyses show that sand is covering most parts of Area 2, and in the close vicinity of the dry-season channel it is in almost all cases a pure sand. Only one sample is classified as sandy gravel. The two boreholes show the sand in the wet-season channel and on the river flanks is often mixed with silt and clay. This is probably due to seasonal changes in water velocities.

In all three resistivity profiles from Area 2, four different layers can be identified. The topmost 5-15 m thick medium to high resistivity layer (37-1400 Ωm) consists of alluvial sand, changing from very dry sand at the surface into more moist sand further down. This was confirmed visually during the field work, from grain size analyses and by the augering. Due to vegetation growing on the river flanks and within the wet-season channel, the topmost part of this sand layer is often mixed with organic matter. According to the surface and borehole soil samples silt and clay is also mixed into the sand at some locations. Between the years the wet-season channel is probably varying in areal extent, depending on the amount of water, and this is probably the reason for the mixing of sand and finer sediments at the margins of the channel and on the nearest parts of the river flanks.

Underlying the topmost sand layer in the long profile and the downstream cross profile 2_3 is a thin discontinuous layer (5-10 m) of low resistivity (8.8-37 Ωm), which most likely consists of fine alluvial sediments (clay and silt). The sediments have most likely been deposited during stages with lower water velocities in high flood seasons. In the upstream cross profile 2_2 this layer is clearly visible in the SSW part. It is more diffuse if this layer is present in the NNE part of the profile, but there are some indications, e.g. around 300 m and 500 m, which indicates that it is most likely present throughout the entire profile.

A third medium resistivity (18-160 Ωm) layer is present in all profiles. In the long resistivity profile this layer thickens in a downstream direction, from ~10 m to 30-40 m, which is confirmed by the two cross profiles. In the SSW part of the upstream cross profile, where it crosses the long profile, this layer is ~5-10 m thick, while it is about 30 m thick in the downstream cross profile. The resistivity values indicate that this layer probably consists of saturated sand or sand mixed with

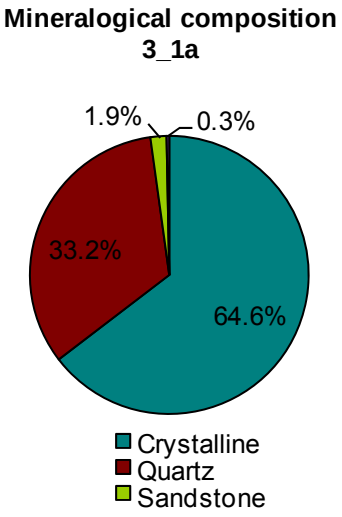

Fig. 24. Pie chart displaying the mineralogical composition for sample 3_1a in percentages of total amount of counted grains.

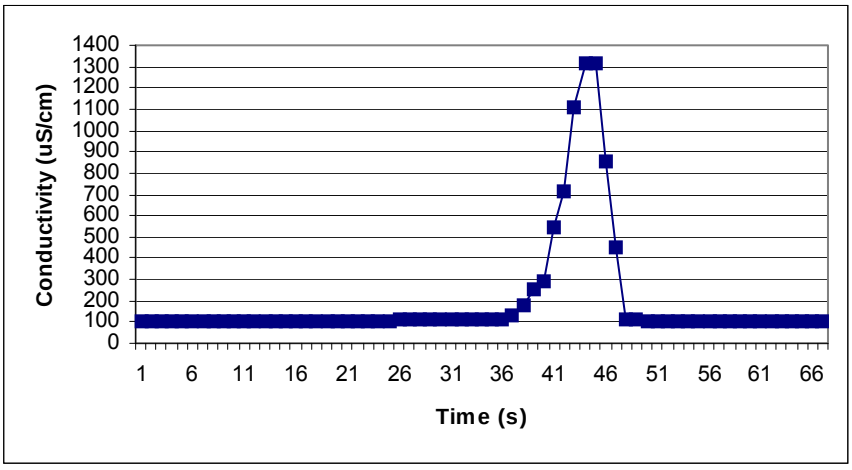

Fig. 25. Graph showing the relation between conductivity in µS/cm and time in seconds (s) for the dry-season channel in Area 3.

some finer material. It seems likely these sediments are alluvial and that they were deposited by the river when it reached the rift margin and the Rift valley floor.

The bottommost layer present in the profiles is another low resistivity (1-18 Ωm) layer. This layer most likely consists of a saturated sandstone with a high porosity, possibly the Sena or Lupata sandstones, or both. These sandstones are present north and south of the area. Both collected rock samples from the Sena sandstone outcrops were classified as arcosic sandstone and the occurring white precipitation is most likely kaolin-weathered feldspar. The samples were found to be poorly consolidated, confirming a high porosity of the sandstone layer.

Vertical extended heterogeneities are visible in the resistivity models, and the upper layer boundary of the bottommost layer is displaying horizontal irregularities (Appendix 2A). These heterogeneities and irregularities are somewhat diffuse, but due to the sandstone being located on a rift margin they most likely indicate the presence of several small faults and displacement features. The upper layer boundary seems to be gently dipping in a downstream direction, which is confirmed by both cross profiles. This dip could be a visual effect related to the small faults and displacement features. In the geological map (DNG 2006) the sandstones causes a narrowing of the river valley at the location of Area 2. This narrowing seems to separate the great alluvial plain on the Rift valley floor from a small basin west of the narrowing.

Another possible interpretation of the resistivity profiles could be that the repeated faulting of the sandstone have caused the alluvial sediments to form wedges of coarse sediments fining upwards (Fig. 26). However, in the case of this alternative interpretation the hydrology would most likely not be affected since the sandstone in both cases is most likely heavily fractured and porous, and have a high permeability.

The mean residuals in the IP models are high, ranging from 22.0 % to 45.1 %. These high percentages of error are too high for the models to be used as a base for interpretation. The downstream cross profile (2_3) has the lowest percentage of error. This IP model is very homogenous and no IP effects are visible, which could indicate that the interpretation of the resistivity model is correct since neither sand, nor sandstone, would give rise to any IP effects. But since the percentage of error still is to high this can not be undoubtedly concluded. The reason for the high error percentages are further described in chapter 6.4 (Sources of error), but is basically depending on poor electrode contact during the measurements.

6.2 Area 3

The grain size analyses show medium to coarse sand covers both the dry- and the wet-season channels. On the northern river flank, borehole BH2 shows the topmost 3.5 m of sand is mixed with some silt and clay.

In all three resistivity profiles from Area 3, three different layers can be identified. The topmost 5-10 m thick medium to high resistivity (37-1400 Ωm) layer consists of alluvial sand, changing from very dry sand at the surface into more moist sand further down. This was visually confirmed during the field work, from the grain size analyses and by the augering. Due to vegetation growing on the flanks, and in some areas also within the wet-season channel, the top layer is here mixed with some organic matter. According to the surface soil samples and the soil samples from borehole BH2, silt and clay is also mixed into the sand at some locations. Between the years the wet-season channel is probably varying in areal extent depending on the amount of water, and this is probably the reason for the mixing of sand and finer sediments at the margins of the channel and on the nearest parts of the river flanks.

The underlying layer is a discontinuous 5-8 m thick layer with low resistivities (1-18 Ωm) in all three resistivity profiles. These low resistivity values indicate that the layer consists of fine alluvial sediments (clay and silt), deposited during stages with lower water velocities in high flood seasons. Borehole BH2 reaches just over four metres depth and at this depth a

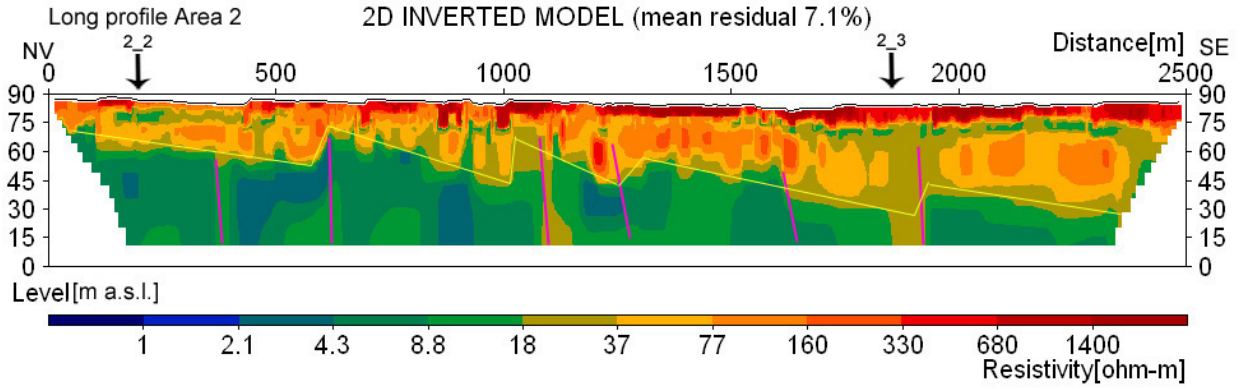

Fig. 26. Two-dimensional resistivity model for the long profile in Area 2. Marked by pink lines are suggested major faults and the yellow lines marks wedges of coarse sediments fining upwards. The black line at the top of the sections represents the levelled ground surface.

thin layer of highly consolidated silty clayey sand is present. It is possible that this thin layer represents the upper boundary of the finer grained sediments.

Below the low resistivity layer a 45-50 m thick layer of low to medium resistivities (2.1-77 Ωm) is visible. The resistivity values indicate that this thick layer consists of saturated sandy sediments mixed with some finer material (silt and clay). The river is flowing in an incised valley in the western part of the Rift valley floor sedimentary fill and it seems likely that this layer consists of alluvial sediments, deposited by the river.

Bottommost in the resistivity profiles very low resistivities are indicating that another layer is present below the sandy sediments. Most likely this layer consists of sandstone of either/or Lupata and Sena sandstones.

The mean residuals in the IP models are 157.6 %, 403.7 % and 22.8 %. These high percentages of error are, in at least the two former cases, far too high for the models to be used as a base for interpretation. The downstream cross profile (3_3) has the lowest percentage of error. This IP model is, in accordance with the downstream cross profile (2_3) in Area 2, very homogenous and no IP effects are visible. This could indicate that the interpretation of the resistivity model is correct since neither sand, nor sandstone, would give rise to any IP effects. But since the percentage of error still is to high this can not be undoubtedly concluded. The reason for the high error percentages are further described in chapter 6.4 (Sources of error), but is basically depending on poor electrode contact during the measurements.

6.3 Combining and comparison of the two areas

The resistivity values are in general slightly lower in Area 3 than in Area 2, which means the alluvial fill becomes less resistive in a downstream direction. This could be related to the sediments becoming finer while moving away from the rift margin. But since no reference material is available from deeper layers, it can not for certain be confirmed this being the case. The surface and borehole soil samples show the coarsest material in Area 2 is sandy gravel and gravelly sand, while coarse sand is the coarsest material in Area 3. This variation in grains size most probably only reflects channel natural discharge variations and not distance from the rift margin.

Sediment samples from boreholes in Area 2 display both angular and rounded particles. This indicates variation in transportation distances of the material. The mineralogical composition of the close-to-surface soil show little variation, both within Area 2 and between the two areas, suggesting the material in all five samples have the same origin. All samples are predominated by crystalline fragments, and since the river is flowing in an east/southeast-ward direction, this material most likely originates from the crystalline basement (Báruè Supergroup) of the Báruè Platform. The sample from borehole BH2 contains the highest amount of sandstone grains, which is to be expected with respect to its location close to the sandstone outcrops. The lowest amounts of sandstone grains are in samples 2_1b and 3_1a, which seems reasonable since they are both located in the middle of the wet-season channel where the most substantial transportation takes place. According to Lächelt (2004) and Tinley (1977) the sandstone is calcareous, but the carbonate content analyses showed that both the sandstone samples and the soil samples contained ≤5% carbonate. This neither contradicts nor confirm that a part of the grains in the soil samples originate from the sandstone. The few percentages of volcanic rock fragments present might originate from the phonolitic lava of the Lupata Formation. This formation is present both next to the Nhandugue River at the western end of Area 2 and next to the Muche River, which is joining the Nhandugue River just west of Area 2.

Figure 27 is a schematic block model of the interpreted geology in Areas 2 and 3. The three topmost layers in Area 2 correspond to the three layers distinguished in Area 3 (Fig. 27). Indicated by very low resistivities in the bottom of the resistivity profiles from Area 3 the bottommost layer of sandstone in Area 2 is most likely present below the bottommost alluvial sediments in Area 3 (Fig. 27). In both cases the topmost layer consists of sands with a relatively high hydraulic conductivity. Due to the layer being in direct contact with the atmosphere it constitutes an unconfined aquifer (Fig. 27). The calculated values on hydraulic conductivity range from 0.22×10^{-3} m/s to 2.45×10^{-3} m/s in Area 2 and from 0.46×10^{-3} m/s to 1.18×10^{-3} m/s in Area 3 which is well within the limits of unconsolidated sands according to Cherry & Freeze (1979): hydraulic conductivity for unconsolidated clean sands is 10^{-6} - 10^{-2} m/s and 10^{-7} - 10^{-4} m/s for silty sands.

The underlying finer sediments are discontinuously distributed in both areas, forming an aquiclude through which there is a possibility for leakage in a downward direction (Fig. 27). In Area 2 the third layer from the top is thickening in downstream direction, from ~10 m to ~30-40 m, and in Area 3 this layer becomes even thicker (~50 m) (Fig. 15 and 21, Appendix 2). The layer most likely consists of permeable sediments, hence forming a semi-confined aquifer. The bottommost sandstone layer present in Area 2 and indicated in Area 3 shows very low resistivities, indicating high porosity and water-saturated conditions. Several small water filled-fracture zones are also most likely present due to heavy faulting. Hence, the layer is forming a semi-confined pore aquifer (Fig. 27).

An east/southeast-ward flow direction of the river together with the gently dip of the sandstone layer is indicating a hydraulic groundwater gradient towards the Rift valley floor. This direction is also indicated by the gently east/southeast-sloping ground surface.

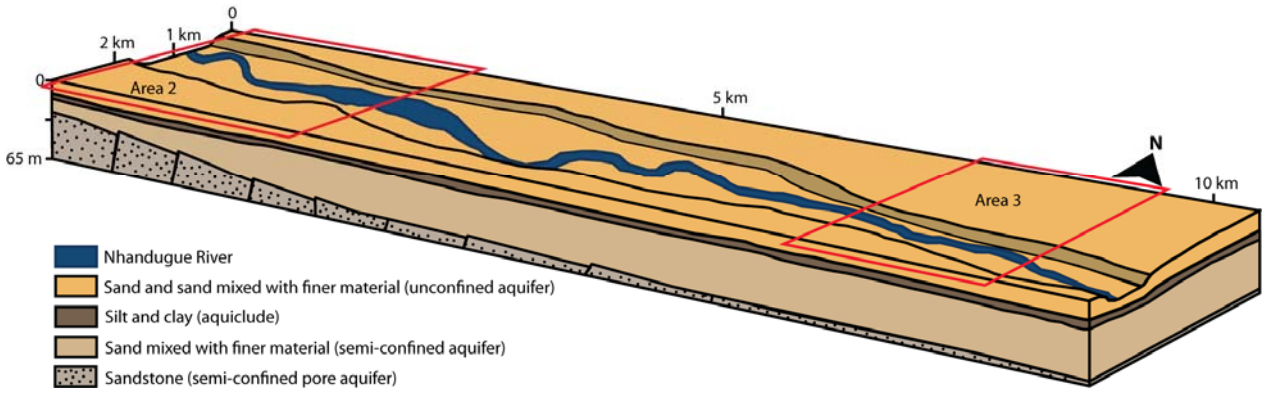

Fig. 27. Schematic block model of the geology in Area 2 and 3. Areas 2 and 3 are marked by red rectangles; Area 2 to the left and Area 3 to the right. All scales and the extent and location of the different morphological units, i.e. the dry-season channel, wet-season channel and the river flanks, are somewhat approximate. Four different layers and also four different aquifers/ aquicludes can be distinguished; (i) a topmost layer of sand, (ii) a second layer of finer sediments, (iii) a layer of sand, mixed with some finer material and, (iv) a layer of sandstone which is faulted.

The water discharge is changing from 214 L/s in Area 2 to 74 L/s in Area 3. Hence, there is a loss in surface water downstream. In field it could also be concluded that the Nhandugue River channel became dry about 14-15 km downstream of Area 3. As mentioned above the stratigraphy of the area makes it possible for water to infiltrate from the surface to deeper layers. It is therefore suggested that this lost surface water is in parts evapotranspirated and in parts infiltrating downwards, forming groundwater in the lowermost layers. To sum up, it can be confirmed that the rift margin is a likely groundwater recharge zone and the probable east/southeast-ward hydraulic groundwater gradient indicate that groundwater flows towards and feeds Lake Urema.

6.4 Sources of error

During the collection of resistivity and IP data it was concluded that the contact between the electrodes and the ground was very poor due to the very dry and often coarse material at the surface. Water was poured on the electrodes and small pits were dug to increase the contact, but negative resistivities were still a significant problem. The poor ground contact also lead to serious data quality problems for the IP data due to capacitive coupling in the multi-conductor cables. The long profile in Area 3 was the first profile to be measured and here the problems were especially large. This was, except for the poor ground contact, due to one of the five multi-conductor cables, used to speed up the roll-along procedure, which had takeouts that were not working properly. During the processing of data, as many bad data points as possible were removed, but the quality of the data set for some of the profiles were still not very good. For some of the profiles very few data points were remaining at some depths, causing the inversion of the data to be less reliable at these depths.

For the elevation surveying the only available levelling equipment was very basic and during the measurements several problems were faced. The string used was slightly elastic, which caused the distances between the measuring sticks to slightly vary and the string to slacken due to the weight of the clinometer. The measuring sticks had a small diameter, which made them sink into the soft ground at some locations, causing alterations in the fixed height above ground. Another difficulty was to place the measuring sticks in an absolutely correct angle (90°) in relation to the ground, due both to the elasticity of the string and to the softness of the ground. Subjectivity was a problem during readings of the clinometer, since the weight was not directed straight down and the low numbers had been almost completely erased. For the regular compass used to get the orientation of the profile, the needle was sluggish and not rotating properly. Especially slow was the needle if the compass was not stored horizontal. All these sources of error during the measurements contributed to inaccuracies in the calculated height difference values, making it necessary to correct this for one of the profiles.

For the geological ground truthing a few sources of error can be highlighted. During the hand-held augering no casing was used to stabilize the borehole walls. In cases where the soils were coarse and dry, some of the material from the walls fell into the hole. When the groundwater level was reached the material in the bottom of the hole was unstable and collapsed. Therefore there is a risk of some samples being contaminated by soil from other layers, and also a risk that the bottommost samples in some cases are in fact samples from the same depths.

Before the transportation of the samples to Sweden, they were split in order to minimize the weight. Due to this splitting there is a small risk the composition of some samples might have been slightly altered from the natural composition. For the hydrometer analyses the sample weight used was settled to ~100 g according to expected low clay content.

Based on the results, the clay content was higher than expected in some cases and therefore smaller samples should have been used for the analysis. Another source of error during the hydrometer analyses are the readings during the first couple of minutes after the hydrometer was placed in the mixture. During this time the hydrometer was bobbing up and down, making it hard to do readings.

7 Conclusions

- Three different layers of Quaternary sediments are present in the two areas: (i) a topmost layer of sand, (ii) a second layer of finer sediments and, (iii) a layer of sand mixed with some finer material. The thickness of the topmost and the second layer are 5-15 m and 5-10 m, respectively. The third layer is thickening in downstream direction, from ~10 m to ~50 m. All Quaternary sediments are alluvial deposits, which most likely have been deposited by the river.
- A slight decrease in the resistivity values can be seen in downstream direction, indicating the sediments becoming finer when moving away from the rift margin. The grain sizes and mineralogical composition of the samples can not clearly confirm the sediments becoming finer. Instead these properties seem to vary depending on where in the river valley they have been deposited.
- A layer of most likely sandstone of either, or both, Sena Formation and Lupata Group is probably underlying the Quaternary sediments. The layer is gently dipping to the east/southeast, causing an east/southeast-ward hydraulic gradient.
- Three different aquifers and one aquiclude can be distinguished. The bottommost sandstone and the overlying sandy sediments form two major semi-confined aquifers, while the topmost sand layer forms a 5-15 m thick unconfined aquifer. The finer sediments in between the sandy sediments are forming a 5-10 m thick aquiclude.
- The surface water discharge is 214 L/s in Area 2 and 74 L/s in Area 3, i.e. the river discharge decreases in downstream direction.
- The thin aquiclude present is an in part permeable layer. This makes it possible for surface water to infiltrate to the deeper aquifers and to be transported as groundwater in an east/southeast-ward direction.
- The hydrogeological conditions confirm that the rift margin is a likely groundwater recharge zone. The east/southeast-ward hydraulic groundwater gradient further suggests groundwater is flowing towards, and feeds, Lake Urema.

8 Recommendations

For continued work along the western rift margin it is recommended to do water chemistry analyses on river water, groundwater and the water in Lake Urema, in order to determine whether some of the water in Lake Urema is truly originating from the Nhandugue River or not. To get more representative and statistical values on discharge it is also recommended to repeat and, preferably, to do continuous dilution tests.

To properly confirm the interpretation of the resistivity profiles it is recommended to drill at least one borehole to a depth of at least 60 m. It is suggested to place this borehole in the middle of area two in order to reach what has been interpreted to be sandstone. This borehole could then be used for collecting continuous data on changing groundwater levels and for sampling water for chemistry analyses. In order for a better mapping of the groundwater flow and the hydraulic gradient there is a need for a number of drilled wells. From such an observation net it would be possible to do more proper groundwater recharge calculations.

The obtained two-dimensional images of the subsurface across the Urema Rift are only a start; it is recommended to continue with additional resistivity profiles. One interesting location would be the floodplain north of Lake Urema. Other interesting locations are the eastern rift margin and the area at which the Vunduzi River flows on to the Rift valley floor at the western rift margin. The Vunduzi River is supported throughout the year by water from the Gorongosa Mountain.

The problems with poor electrode contact were extensive during conducted field work. For work in areas with dry permeable soils it is recommended to try with mixing starch compound (e.g. Johnson Revert intended to stabilize wells during drilling) into the water that is poured onto the electrode, this to increase the ground contact. This is intended to make the water more viscous and can serve to keep the water in place for a sufficiently longer time according to ABEM (2009). When it comes to collecting reference material for interpretation of resistivity data it is recommended to set the sample depth to ~1 m depth instead of 15-30 cm. This is preferable since the topmost half to one metre of the ground is not included in the resistivity measurements due to the data collecting procedure.

9 Acknowledgements

There are many people I would like to give a special thank to for making it possible to write this thesis. Thank you to:

- Li Stenberg for good partnership during the developing of this thesis and for being a good travel companion during the field trip to Mozambique.
- Franziska Steinbruch, Manager of Scientific Services at Gorongosa National Park, and Dr. Rickard Owen at the Department of Geol-

ogy at the University of Zimbabwe for their guidance and support during the field work period in Mozambique and for answering questions and helping out with interpretation.

- Farisse Chirindja for his support and assistance during the field work and the entire stay in Mozambique and Luís Magaia and Felix Oqueio for their invaluable assistance in field.
- All staff at Gorongosa National Park for their hospitality and helping us out with whatever problems we had and USAID for funding equipment and staff time.
- The Geological Department at Eduardo Mondlane University in Maputo, Mozambique, for use of the department's utilities and for lending us resistivity equipment and a vehicle for the field work.
- SIDA-SAREC for the funding of the research cooperation between Lund University, Eduardo Mondlane University and Gorongosa National Park, and SIDA for the Minor Field Study scholarship that constituted a major part of the funding for this study.
- My supervisors at Lund University, Sweden, Professor Torleif Dahlin at the Department of Engineering Geology and Professor Per Möller at the Department of Earth and Ecosystem Sciences for their support, advises, proofreading and feedback. Per Sandgren, Head of Department for Earth and Ecosystem Sciences, for his encouragement and support.

Last but not least, thank you to all my friends and family for all your encouragement and support.

10 References

ABEM, 2009: *Instruction Manual Terrameter SAS 4000 / SAS 1000*. ABEM Instrument AB, Sundbyberg, Sweden. 136 pp.

Ambrosiani, K.G., 1995. Kompendium i jordartsanalys - laboratorieanvisningar. *QUATERNARIA Ser. B, Nr 1*, Stockholms universitet, Stockholm, Sverige. 128 pp. (in Swedish)

Beilfuss, R., Owen, R. & Steinbruch, F., 2007: *Long-term plan for hydrological research: adaptive management of water resources at Gorongosa National Park*. Report prepared for Gorongosa Research Center, Gorongosa National Park, Mozambique. 26 pp.

Benischke, R. & Harum, T., 1990: Determination of discharge rates in turbulent streams by salt tracer dilution applying a microcomputer system. Comparison with current meter measurements. *In* Lang, H. & Musy, A. (ed) *Hydrology in Mountainous Regions I — Hydrological Measurements; The Water Cycle,* 215-221. IAHS Symposium, Lausanne, 7 August — 1 September 1990. IAHS publications 193.

Bowen, R., 1986: *Groundwater 2nd Edition*. Elsevier Applied Science Publishers, London. 427 pp.

Böhme, B., Steinbruch, F., Gloaguen, R., Heilmeier, H. & Merkel, B., 2006: Geomorphology, hydrology, and ecology of Lake Urema, central Mozambique, with focus on lake extent changes. *Physics and Chemistry of the Earth 31*, 745-752.

Chapuis, R.P., 2004: Predicting the saturated hydraulic conductivity of sand and gravel using effective diameter and void ratio. *Canadian Geotechnical Journal 41*, 787-795.

Cherry, J.A & Freeze, R.A., 1979: *Groundwater*. Prentice-Hall, cop. 604 pp.

Chirindja, F. & Hellman, K., 2009: *Geophysical investigation in a part of Gorongosa National Park in Mozambique – A Minor Field Study*. M.Sc. thesis, Department of Engineering Geology, Lund University, Lund, Sweden. 47 pp.

Dahlin, T., 1993: *On the automation of 2D resistivity surveying for engineering and environmental applications*. Ph.D. thesis, Department of Engineering Geology, Lund University, Lund, Sweden. 187 pp.

Dahlin, T. & Zhou, B., 2006: Multiple-gradient array measurements for multichannel 2D resistivity imaging. *Near Surface Geophysics, vol. 4, no 2*, 113-123.

Gorongosa National Park [GNP], 2009: [homepage] http://www.gorongosa.net/. Assessed 26th of May 2009

Halkjaer, E., 2007: *Länder i fickformat 207 Mocambique/Malawi.* Utrikespolitiska Institutet (The Swedish Institute of International Affairs), Stockholm, Sweden. 40 pp. (In Swedish)

Jeppsson, H., 2009: *Geoelektriska metoder inom til lämpad geofysik - Kompendium i Geofysiska undersökningsmetoder*. GEOC04 kursmaterial, Geologiska Institutionen, Lunds universitets, Lund, Sverige. 56 pp. (in Swedish)

Loke, M.H., 2004: *Tutorial: 2-D and 3-D electrical imaging surveys*. [Available at: http://www-geo.phys.ualberta.ca/~unsworth/UA-classes/223/loke_course_notes.pdf.]

Lächelt, S., 2004: *The geology and mineral resources of Mozambique*. National Directorate of Geology, Maputo, Mozambique. 515 pp.

Merkel, B.J. & Steinbruch, F., 2008: Characterization of a Pleistocene thermal spring in Mozambique. *Hydrogeology Journal 16*, 1655-1668.

Moss, R.H., Watson, R.T. & Zinyowera, M.C., 2001: *The Regional Impacts of Climate Change An Assessment of Vulnerability*. IPPC Special Report, UNEP/GRID-Arendal.

National Directorate of Geology [DNG], 2006: Geological map of Gorongosa, Mozambique. Scale 1:250 000.

Owen, R., 2004: The Millennium Ecosystem Assessment (MA). GM SAFMA Hydrogeology condition and trend report. Mineral Resource Centre, University of Zimbabwe, Zimbabwe.

Reynolds, J.M., 2007: *An introduction to applied and*

environmental geophysics. John Wiley and Sons. 796 pp.

Stenberg, L., 2010: *Geophysical and hydrogeological survey in a part of the Nhandugue river valley, Gorongosa National Park, Mozambique – Area 1 and 2*. M.Sc thesis, Department of Earth and Ecosystem Sciences, Lund University, Sweden.

The CGIAR Consortium for Spatial Information [CGIAR-CSI], 2008: SRTM 90m Digital Ele vation Data [Available at: http://srtm.csi.cgiar. org/]

Tinley, K.L., 1977: *Framework of the Gorongosa eco system*. Ph.D. thesis, Faculty of Science, Uni versity of Pretoria, Pretoria, South Africa. 184 pp.

United Nations Environment Programme [UNEP], 2002: *African Environment Outlook Past, pre sent and future perspectives*. UNEP/GRID-Arendal.

Appendix 1

Geological map over the Urema Rift.
The red rectangle marks the study area.
The map is adapted from DNG (2006).

REPÚBLICA DE MOÇAMBIQUE
MINISTÉRIO DOS RECURSOS MINERAIS
DIRECÇÃO NACIONAL DE GEOLOGIA

GORONGOSA

FOLHA Nº 1834

SÉRIE GEOLÓGICA 1:250 000

Base topográfica: **Consórcio GTK**
Projecção: U.T.M.; Elipsóide: WGS84
Unidades: Metros; Datum: Moznet 36S
Coordenadas: U.T.M. - Zona 36

Referência
Elevação digital do SRTM / Modelos numéricos de elevação
Dados relativos à elevação: U.S. Geological Survey, 2003
Missão topográfica do Shuttle Radar (SRTM)
USGS web site: http://srtm.usgs.gov/ (2003-2004)
Disponível através de: USGS web site. Acesso em: 2004-2005
Resolução espacial: 90 metros
Unidade de altitude: Metros
Datum: WGS84

Escala 1:250 000

0 5 10 20 30 km

Data da versão final: 30 de Novembro de 2006

MINERAL RESOURCES MANAGEMENT CAPACITY BUILDING PROJECT
Component 2: Geological Infrastructure Development Project: Geological Mapping (LOT 2)

NDF Credit 335

Consórcio GTK para Cartografia Geológica

GTK - ITC - GONDWANA - SGU - GEUS

Compilação de / Compiled by: M. Ferrara e T. Manninen, 2005

Levantamento geológico efectuado por / Mapped by:. M. Ferrara, T. Manninen e T. Lehto, E. Korkiakoski (Depósitos Minerais / Mirieral Resources)

Cartografia digital realizada por / Digital cartography: H. Saastamoinen e A. Lindh

Notícia Explicativa / Map Explanation, Volume 2

LEGENDA
LEGEND

Supergrupo / *Suite* / COMPLEXO Supergroup / *Suite* / COMPLEX	Grupo Group	Formação Formation	ROCHAS SEDIMENTARES, VULCÂNICAS E COMPLEXOS METAMÓRFICOS SEDIMENTARY, VOLCANIC ROCKS AND METAMORPHIC COMPLEXES	ROCHAS PLUTÓNICAS E DIQUES PLUTONIC ROCKS AND DYKES
			Qa — Alluvium, sand, silt, gravel	
			Qps — Eluvial floodplain clayey sand	
			Qc — Colluvium	
		Mazamba	TrM — Arkosic sandstone, in part conglomeratic	
			TrZ — Inhaminga Sandstone	
		Cheringoma	TrC — Limestone, glauconitic sandstone	
		Grudja	CrG — Marl, silt, limestone, gypsum	
		Sena	CrSb — Basal Conglomerate Member; conglomeratic sandstone	
			CrSt — Thorium sandstone Member; conglomeratic sandstone (high Th signature)	
Xiluvo				*Xiluvo Suite*: CrXq — Quartz lens, commonly brecciated
				Xiluvo Suite: CrXa — Alkaline intrusion
	Lupata	Monte Linhanga	CrLM — Phonolitic lava	
		Monte Mazambulo	JrLM — Conglomerate sandstone	
		Chueza	JrC — Amygdaloidal basalt	
Gorongosa				*Gorongosa Suite*: JrGg — Granite, syenitic (181±1 Ma magmatic U/Pb)
				Gorongosa Suite: JrGb — Gabbro
				md — Mafic dyke
Karoo	Upper Karoo	Serra Bombuè	JrSb — Rhyodacite and rhyolite	
		Rio Nhavúdezi	JrRN — Amygdaloidal basalt	
				fd — Felsic dyke
	Cádzi		PeC — Arkosic sandstone, conglomerate and limestone beds	
				Pgr — Granite and pegmatite
BÁRUÈ				P₂BMg — Monte Tomonda leucocratic gneiss, garnetiferous
				P₂BMgb — Gabbro, gabbroic rock
				P₂BMh — Hornblendite
	Macossa		P₂BMcc — Calc-silicate gneiss, skarn	
			P₂BMsi — Garnet-sillimanite gneiss, mica gneiss, metagreywacke	
			P₂BMfq — Feldspathic quartzite, garnetiferous	
	Chimoio		P₂BCmi — Migmatitic paragneiss	
			P₂BCh — Monte Chissui Gneiss; felsic biotite gneiss, metagranite	

FANEROZÓICO/PHANEROZOIC

Quaternário Quaternary	1.81 Ma
Terciário Tertiary	66 Ma
Cretácico Cretaceous	146 Ma
Jurássico Jurassic	200 Ma
Triássico Triassic	251 Ma
Pérmico Permian	299 Ma

PROTEROZÓICO/PROTEROZOIC

NEOPROTEROZÓICO NEOPROTEROZOIC	542 Ma
MESOPROTEROZÓICO MESOPROTEROZOIC	1000 Ma
	1600 Ma

ARCAICO / ARCHAEAN — 2500 Ma

Appendix 2

Resistivity models from Area 2 and 3. (A) Long profile Area 2, (B) Upstream cross profile 2_2, (C) Downstream cross profile 2_3, (D) Long profile Area 3, (E) Upstream cross profile 3_2 and (F) Downstream cross profile 3_3. Outlined in black are the different layers. The dashed line in (B) indicates uncertain layer division. Indicated by pink vertical lines are faults and displacement features. The black line at the top of the sections represents the levelled ground surface and the blue lines marks the location of the dry-season channel.

(A)

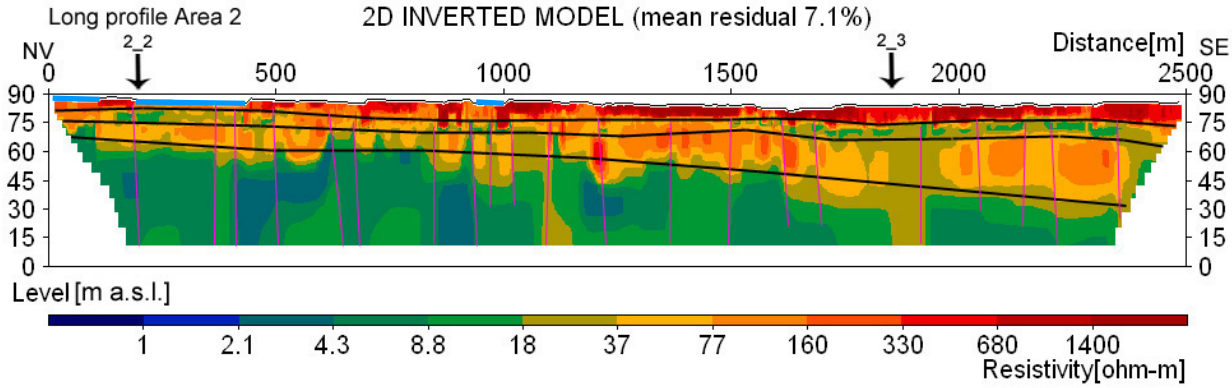

(B)

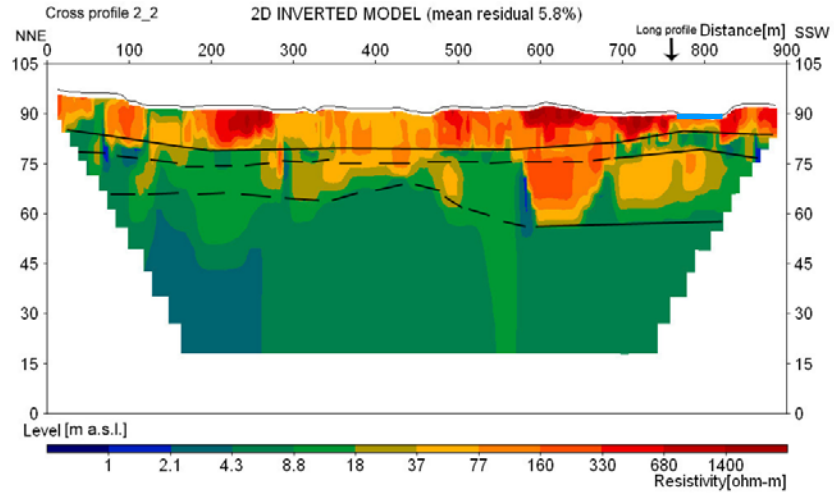

(C)

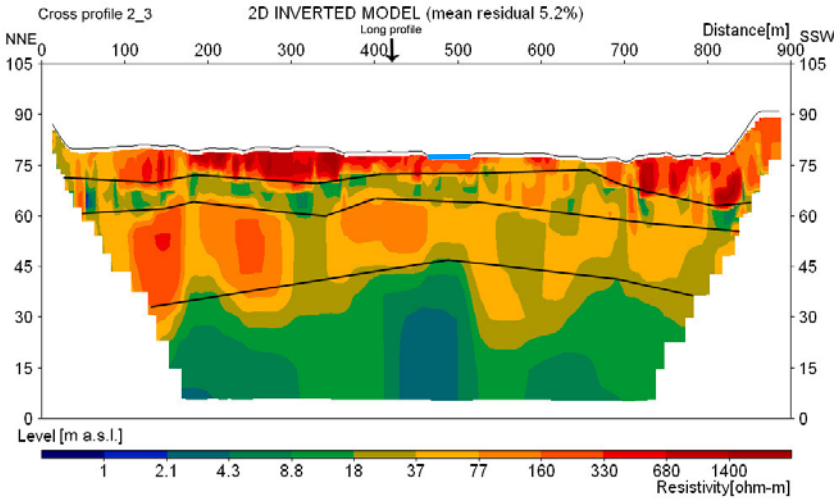

(D)

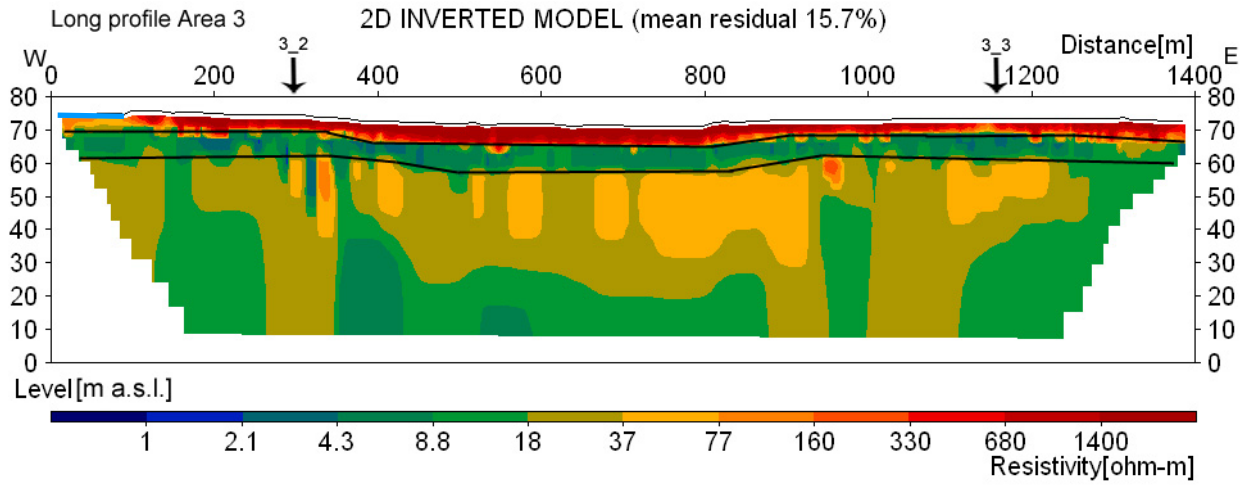
Long profile Area 3
2D INVERTED MODEL (mean residual 15.7%)
W
E
3_2
3_3
Distance[m]
0
200
400
600
800
1000
1200
1400
80
70
60
50
40
30
20
10
0
Level [m a.s.l.]
1
2.1
4.3
8.8
18
37
77
160
330
680
1400
Resistivity[ohm-m]

(E)

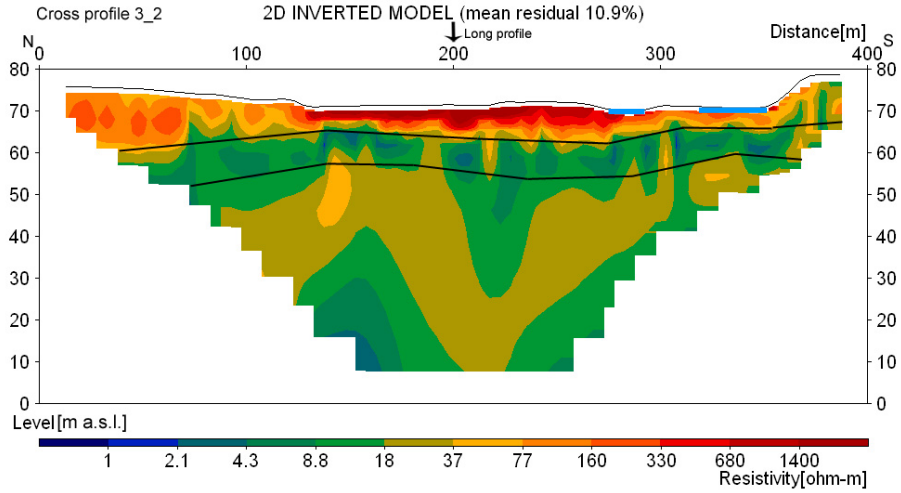
Cross profile 3_2
2D INVERTED MODEL (mean residual 10.9%)
Long profile
N
S
Distance[m]
0
100
200
300
400
80
70
60
50
40
30
20
10
0
Level [m a.s.l.]
1
2.1
4.3
8.8
18
37
77
160
330
680
1400
Resistivity[ohm-m]

(F)

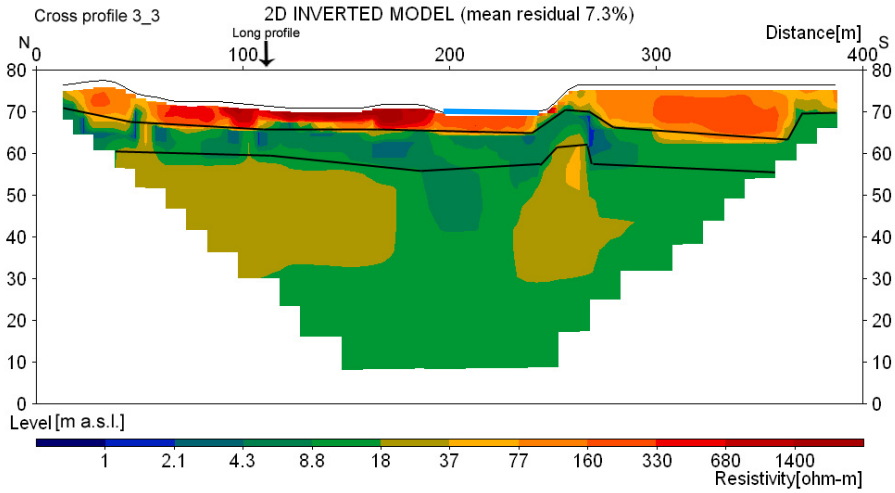
Cross profile 3_3
2D INVERTED MODEL (mean residual 7.3%)
Long profile
N
S
Distance[m]
0
100
200
300
400
80
70
60
50
40
30
20
10
0
Level [m a.s.l.]
1
2.1
4.3
8.8
18
37
77
160
330
680
1400
Resistivity[ohm-m]

Appendix 3

IP models from Area 2 and 3. (A) Long profile Area 2, (B) Upstream cross profile 2_2, (C) Downstream cross profile 2_3, (D) Long profile Area 3, (E) Upstream cross profile 3_2 and (F) Downstream cross profile 3_3. The black line at the top of the sections represents the levelled ground surface.

(A)

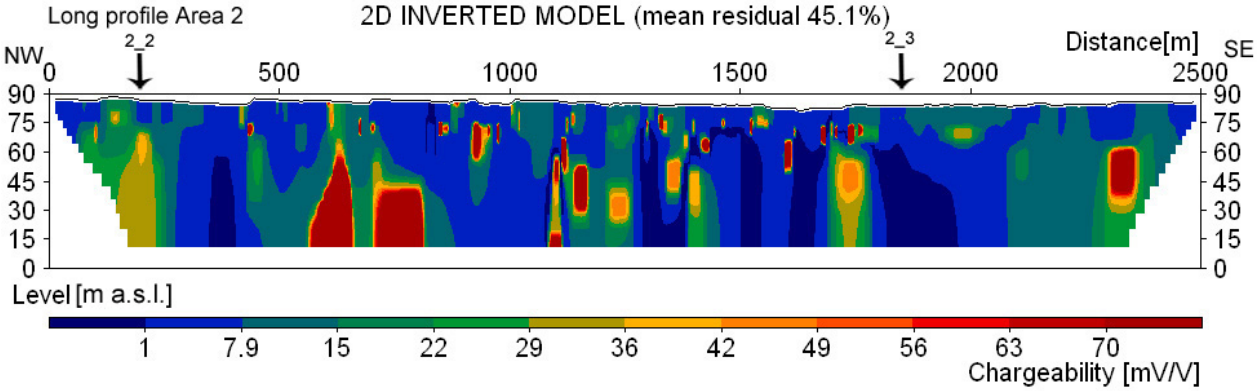

(B)

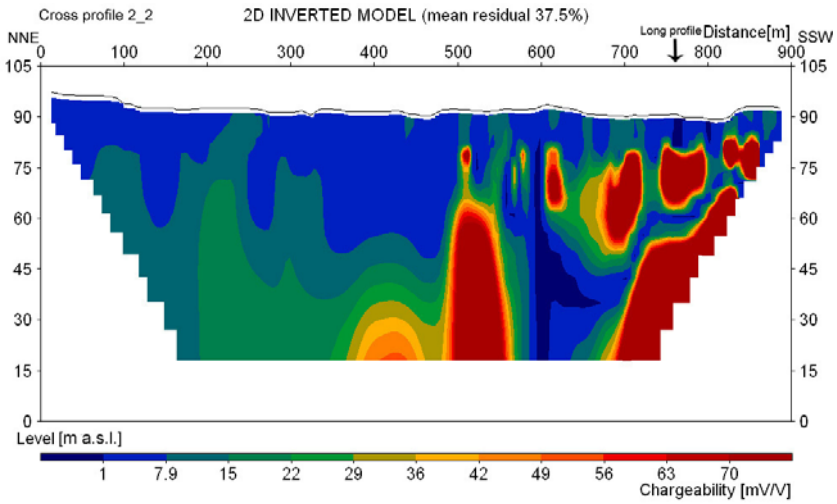

(C)

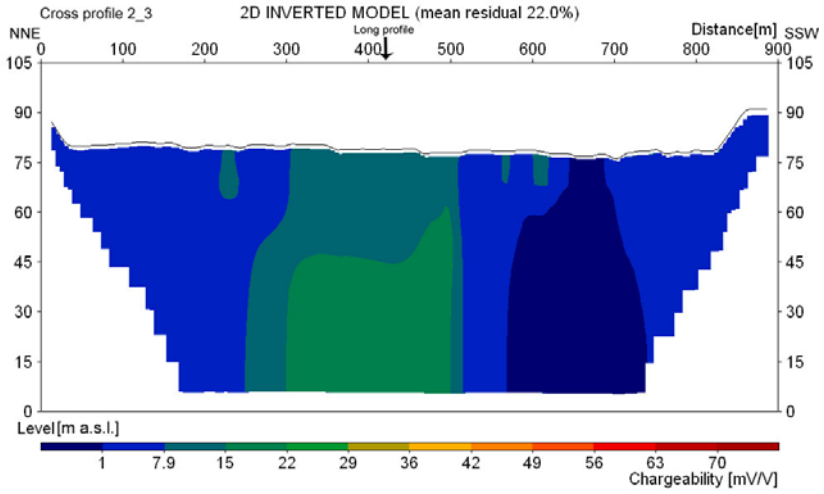

(D)

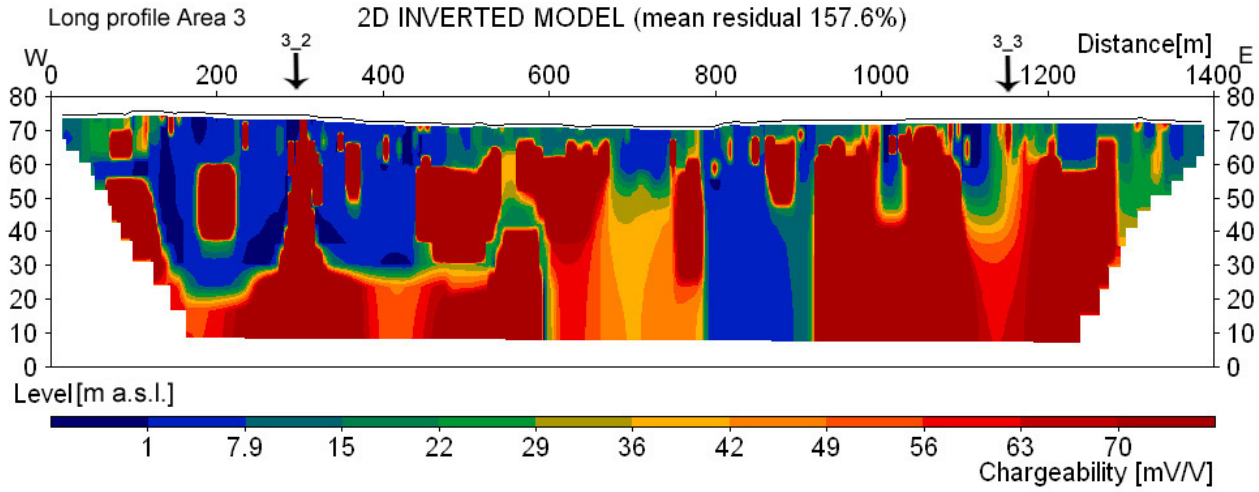
Long profile Area 3
2D INVERTED MODEL (mean residual 157.6%)
3_2
3_3
Distance[m]
W
E
0
200
400
600
800
1000
1200
1400
80
70
60
50
40
30
20
10
0
Level[m a.s.l.]
1
7.9
15
22
29
36
42
49
56
63
70
Chargeability [mV/V]

(E)

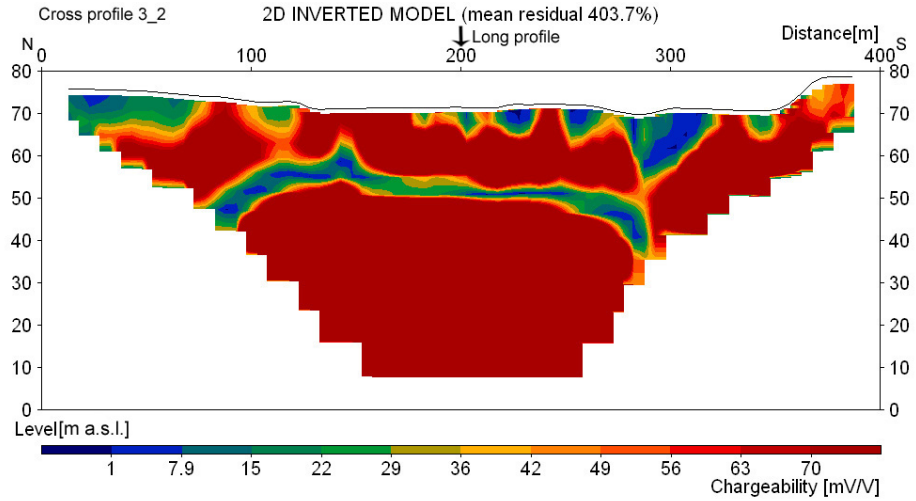
Cross profile 3_2
2D INVERTED MODEL (mean residual 403.7%)
Long profile
Distance[m]
N
S
0
100
200
300
400
80
70
60
50
40
30
20
10
0
Level[m a.s.l.]
1
7.9
15
22
29
36
42
49
56
63
70
Chargeability [mV/V]

(F)

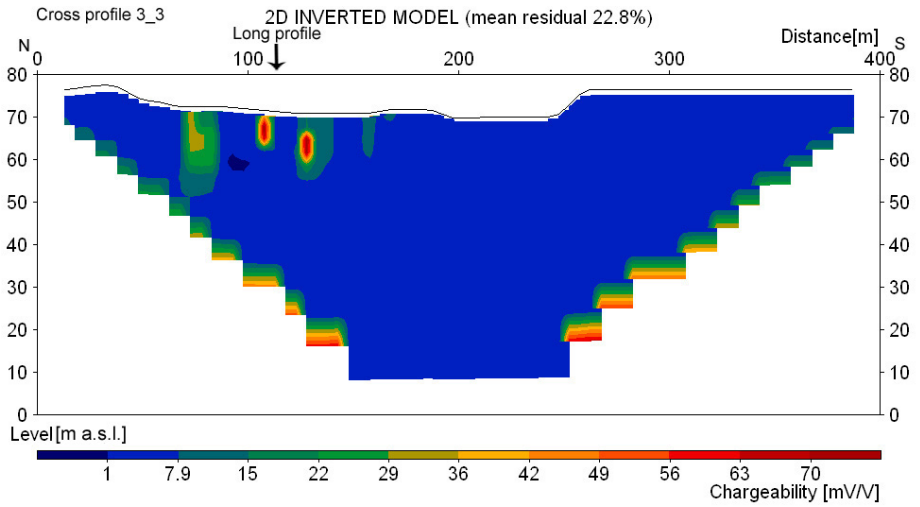
Cross profile 3_3
2D INVERTED MODEL (mean residual 22.8%)
Long profile
Distance[m]
N
S
0
100
200
300
400
80
70
60
50
40
30
20
10
0
Level[m a.s.l.]
1
7.9
15
22
29
36
42
49
56
63
70
Chargeability [mV/V]

Tidigare skrifter i serien ”Examensarbeten i Geologi vid Lunds Universitet”:

240. Bjärnborg, Karolina, 2009: The copper sulphide mineralization of the Zinkgruvan deposit, Bergslagen, Sweden. (45 hskp)
241. Stenberg, Li, 2009: Historiska kartor som hjälp vid jordartsgeologisk kartering – en pilotstudie från Vångs by i Blekinge. (15 hskp)
242. Nilsson, Mimmi, 2009: Robust U-Pb baddeleyite ages of mafic dykes and intrusions in southern West Greenland: constraints on the coherency of crustal blocks of the North Atlantic Craton. (30 hskp)
243. Hult, Elin, 2009: Oligocene to middle Miocene sediments from ODP leg 159, site 959 offshore Ivory Coast, equatorial West Africa. (15 hskp)
244. Olsson, Håkan, 2009: Climate archives and the Late Ordovician Boda Event. (15 hskp)
245. Wollein Waldetoft, Kristofer, 2009: Svekofennisk granit från olika metamorfa miljöer. (15 hskp)
246. Månsby, Urban, 2009: Late Cretaceous coprolites from the Kristianstad Basin, southern Sweden. (15 hskp)
247. MacGimpsey, I., 2008: Petroleum Geology of the Barents Sea. (15 hskp)
248. Jäckel, O., 2009: Comparison between two sediment X-ray Fluorescence records of the Late Holocene from Disko Bugt, West Greenland; Paleoclimatic and methodological implications. (45 hskp)
249. Andersen, Christine, 2009: The mineral composition of the Burkland Cu-sulphide deposit at Zinkgruvan, Sweden – a supplementary study. (15 hskp)
250. Riebe, My, 2009: Spinel group minerals in carbonaceous and ordinary chondrites. (15 hskp)
251. Nilsson, Filip, 2009: Föroreningsspridning och geologi vid Filborna i Helsingborg. (30 hskp)
252. Peetz, Romina, 2009: A geochemical characterization of the lower part of the Miocene shield-building lavas on Gran Canaria. (45 hskp)
253. Åkesson, Maria, 2010: Mass movements as contamination carriers in surface water systems – Swedish experiences and risks.
254. Löfroth, Elin, 2010: A Greenland ice core perspective on the dating of the Late Bronze Age Santorini eruption. (45 hskp)
255. Ellingsgaard, Óluva, 2009: Formation Evaluation of Interlava Volcaniclastic Rocks from the Faroe Islands and the Faroe-Shetland Basin. (45 hskp)
256. Arvidsson, Kristina, 2010: Geophysical and hydrogeological survey in a part of the Nhandugue River valley, Gorongosa National Park, Mozambique. (45 hskp)
257. Gren, Johan, 2010: Osteo-histology of Mesozoic marine tetrapods – implications for longevity, growth strategies and growth rates. (15 hskp)
258. Syversen, Fredrikke, 2010: Late Jurassic deposits in the Troll field. (15 hskp)
259. Andersson, Pontus, 2010: Hydrogeological investigation for the PEGASUS project, southern Skåne, Sweden. (30 hskp)
260. Noor, Amir, 2010: Upper Ordovician through lowermost Silurian stratigraphy and facies of the Borenshult-1 core, Östergötland, Sweden. (45 hskp)
261. Lewerentz, Alexander, 2010: On the occurrence of baddeleyite in zircon in silica-saturated rocks. (15 hskp)
262. Eriksson, Magnus, 2010: The Ordovician Orthoceratite Limestone and the Blommiga Bladet hardground complex at Horns Udde, Öland. (15 hskp)
263. Lindskog, Anders, 2010: From red to grey and back again: A detailed study of the lower Kundan (Middle Ordovician) ‘Täljsten’ interval and its enclosing strata in Västergötland, Sweden. (15 hskp)
264. Rääf, Rebecka, 2010: Changes in beyrichiid ostracode faunas during the Late Silurian Lau Event on Gotland, Sweden. (30 hskp)
265. Petersson, Andreas, 2010: Zircon U-Pb, Hf and O isotope constraints on the growth versus recycling of continental crust in the Grenville orogen, Ohio, USA. (45 hskp)
266. Stenberg, Li, 2010: Geophysical and hydrogeological survey in a part of the Nhandugue River valley, Gorongosa National Park, Mozambique – Area 1 and 2. (45 hskp)
267. Andersen, Christine, 2010: Controls of seafloor depth on hydrothermal vent temperatures - prediction, observation & 2D finite element modeling. (45 hskp)

268. März, Nadine, 2010: When did the Kalahari craton form? Constraints from baddeleyite U-Pb geochronology and geo-chemistry of mafic intrusions in the Kaapvaal and Zimbabwe cratons. (45 hp)
269. Dyck, Brendan, 2010: Metamorphic rocks in a section across a Svecnorwegian eclogite-bearing deformation zone in Halland: characteristics and regional context. (15 hp)
270. McGimpsey, Ian, 2010: Petrology and lithogeochemistry of the host rocks to the Nautanen Cu-Au deposit, Gällivare area, northern Sweden. (45 hp)
271. Ulmius, Jan, 2010: Microspherules from the lowermost Ordovician in Scania, Sweden – affinity and taphonomy. (15 hp)
272. Andersson, Josefin, Hybertsen, Frida, 2010: Geologi i Helsingborgs kommun – en geoturistkarta med beskrivning. (15 hp)
273. Barth, Kilian, 2011: Late Weichselian glacial and geomorphological reconstruction of South-Western Scania, Sweden. (45 hp)
274. Mashramah, Yaser, 2011: Maturity of kerogen, petroleum generation and the application of fossils and organic matter for paleotemperature measurements. (45 hp)
275. Vang, Ina, 2011: Amphibolites, structures and metamorphism on Flekkerøy, south Norway. (45 hp)
276. Lindvall, Hanna, 2011: A multi-proxy study of a peat sequence on Nightingale Island, South Atlantic. (45 hp)
277. Bjerg, Benjamin, 2011: Metodik för att förhindra metanemissioner från avfallsdeponier, tillämpad vid Albäcksdeponin, Trelleborg. (30 hp)
278. Pettersson, Hanna, 2011: El Hicha – en studie av saltstäppssediment. (15 hskp)
279. Dyck, Brendan, 2011: A key fold structure within a Sveconorwegian eclogite-bearing deformation zone in Halland, south-western Sweden: geometry and tectonic implications. (45 hp)
280. Hansson, Anton, 2011: Torvstratigrafisk studie av en trädstamshorisont i Viss mosse, centrala Skåne kring 4 000 - 3 000 cal BP med avseende på klimat- och vattenståndsförändringar. (15 hp)
281. Åkesson, Christine, 2011: Vegetationsutvecklingen i nordvästra Europa under Eem och Weichsel, samt en fallstudie av en submorän, organisk avlagring i Bellinga stenbrott, Skåne. (15 hp)
282. Silveira, Eduardo M., 2011: First precise U-Pb ages of mafic dykes from the São Francisco Craton. (45 hp)
283. Holm, Johanna, 2011**:** Geofysisk utvärdering av grundvattenskydd mellan väg 11 och Vombs vattenverk. (15 hp)
284. Löfgren, Anneli, 2011: Undersökning av geofysiska metoders användbarhet vid kontroll av den omättade zonen i en infiltrationsdamm vid Vombverket. (15 hp)
285. Grenholm, Mikael, 2011: Petrology of Birimian granitoids in southern Ghana - petrography and petrogenesis. (15 hp)
286. Thorbergsson, Gunnlaugur, 2011: A sedimentological study on the formation of a hummocky moraine at Törnåkra in Småland, southern Sweden. (45 hp)
287. Lindskog, Anders, 2011: A Russian record of a Middle Ordovician meteorite shower: Extraterrestrial chromite in Volkhovian-Kundan (lower Darriwilian) strata at Lynna River, St. Petersburg region. (45 hp)
288. Gren, Johan, 2011: Dental histology of Cretaceous mosasaurs (Reptilia, Squamata): incremental growth lines in dentine and implications for tooth replacement. (45 hp)
289. Cederberg, Julia, 2011: U-Pb baddelyit dateringar av basiska gångar längs Romeleåsen i Skåne och deras påverkan av plastisk deformation i Protoginzonen (15 hp)
290. Wenxing Ning, 2011: Testing the hypothesis of a link between Earth's magnetic field and climate change: a case study from southern Sweden focusing on the 1st millennium BC. (45 hp)

LUNDS UNIVERSITET

Geologiska enheten
Institutionen för geo- och ekosystemvetenskaper
Sölvegatan 12, 223 62 Lund